Journal of Molecular Structure 1238 (2021) 130410

Contents lists available at ScienceDirect

Journal of Molecular Structure

journal homepage: www.elsevier.com/locate/molstr

Elucidation for coordination features of hydrazide ligand under influence of variable anions in bivalent transition metal salts; green synthesis, biological activity confirmed by in-silico approaches

Kholood Alkhamis[a], Fatmah Alkhatib[b], Amerah Alsoliemy[b], Abdulmajeed F. Alrefaei[c], Hanadi A. Katouah[b], Hanan E. Osman[d], Gaber A.M. Mersal[e], Rania Zaky[f], Nashwa M. El-Metwaly[b,f,*]

[a] Department of Chemistry, College of Science, University of Tabuk, Saudi Arabia
[b] Department of Chemistry, Faculty of Applied Science, Umm-Al-Qura University, Makkah, Saudi- Arabia
[c] Department of Biology, Jamoum University College, Umm Al-Qura University, Makkah, Saudi- Arabia
[d] Department of Biology, Faculty of Applied Science, Umm-Al-Qura University, Makkah, Saudi- Arabia
[e] Department of Chemistry, College of Science, Taif University, P.O. Box 11099, Taif 21944, Saudi Arabia
[f] Department of Chemistry, Faculty of Science, Mansoura University, El-Gomhoria Street, Egypt

ARTICLE INFO

Article history:
Received 24 February 2021
Revised 29 March 2021
Accepted 30 March 2021
Available online 8 April 2021

Keywords:
Green synthesis
Dft
Conductometry
Biological activity
Pharmacokinetics
Moe-docking

ABSTRACT

Synthesis of new *N′*- cyclohexylidene-3–hydroxy-2-naphthohydrazide (H_2L) complexes was carried out by ball milling technique in the lack of solvent (green approach) and then characterized by analytical and spectroscopic techniques. The metal salts used for preparations, were varied in their conjugated anions (Cl^-, SO_4^{-2} & OAc^-) to investigate the changes in properties of obtained complexes, by changing anions, even with the same ligand. The ligand was coordinated mainly as monobasic with the metal acetate salts, while a neutral with metal chloride or sulfate salts. Such coordination modes were appeared through bidentate or tridentate towards central metals within different molar ratios (1: 1 or 1:2, M:L). Conductometric study was performed for Co(II) complex to estimate the complex stoichiometry and either formation or association constants, in solution state. DMOL3 program was used *via* DFT/B3LYP method to optimize the studied compounds and to obtain essential quantum parameters. Consequently, we confirmed the coordination of O(11), O(13) and N(16) atoms according to their features appeared in molecular modeling study. In-silico assessment was performed to examine the interaction features of new compounds with pathogenic-DNA, before in-vitro screening. Such assessment was carried out firstly by pharmacophore query within MolPort drug-library to discover the analogues drugs in activity towards DNA proteins. MolPort-007–588–377 and MolPort -000–734–772 were the code numbers of two analogues drugs. Secondly MOE-docking process was executed to explain all interaction features and rank the inhibition activity of complexes. Furthermore, antimicrobial, antioxidant and antitumor activity were investigated for all compounds and Ni(II)-Bis(HL) complex showed excellent antioxidant activity. Whereas, Co(II)-Bis(HL) complex showed excellent cytotoxicity towards liver cancer cells. Finally, the whole characteristics of complexes were changed by changing conjugated anions, even with the same ligand.

1. Introduction

Recently, a class of azomethine-based ligands was gained a wide interest due to its chelating ability *via* multiple coordination modes with transition metal ions as well as their distinguish applications [1]. Also, all hydrazide-based ligands could being effectively synthesized by so simple condensation reaction [2]. Different bivalent metal ion complexes were prepared by a green strategy from 4-aminoantipyrine- based ligand and exhibited effective binding with calf-thymus DNA [3]. A series of Cu(II)-hydrazide complexes were prepared and exhibited a significant intrinsic binding with DNA and anti-inflammatory activity [4]. Macrocyclic Ni(II) and Co(II) complexes were prepared and effectively used as a catalyst for CO_2 reduction [5]. The ligand prepared from propanehydrazide and was used to synthesize bivalent metal ion complexes by green way and most of complexes exhibited biological activity [6]. Salicyladehyde derivative was used to prepare Schiff base ligand and

* Corresponding author.
E-mail address: nmmohamed@uqu.edu.sa (N.M. El-Metwaly).

https://doi.org/10.1016/j.molstruc.2021.130410
0022-2860/

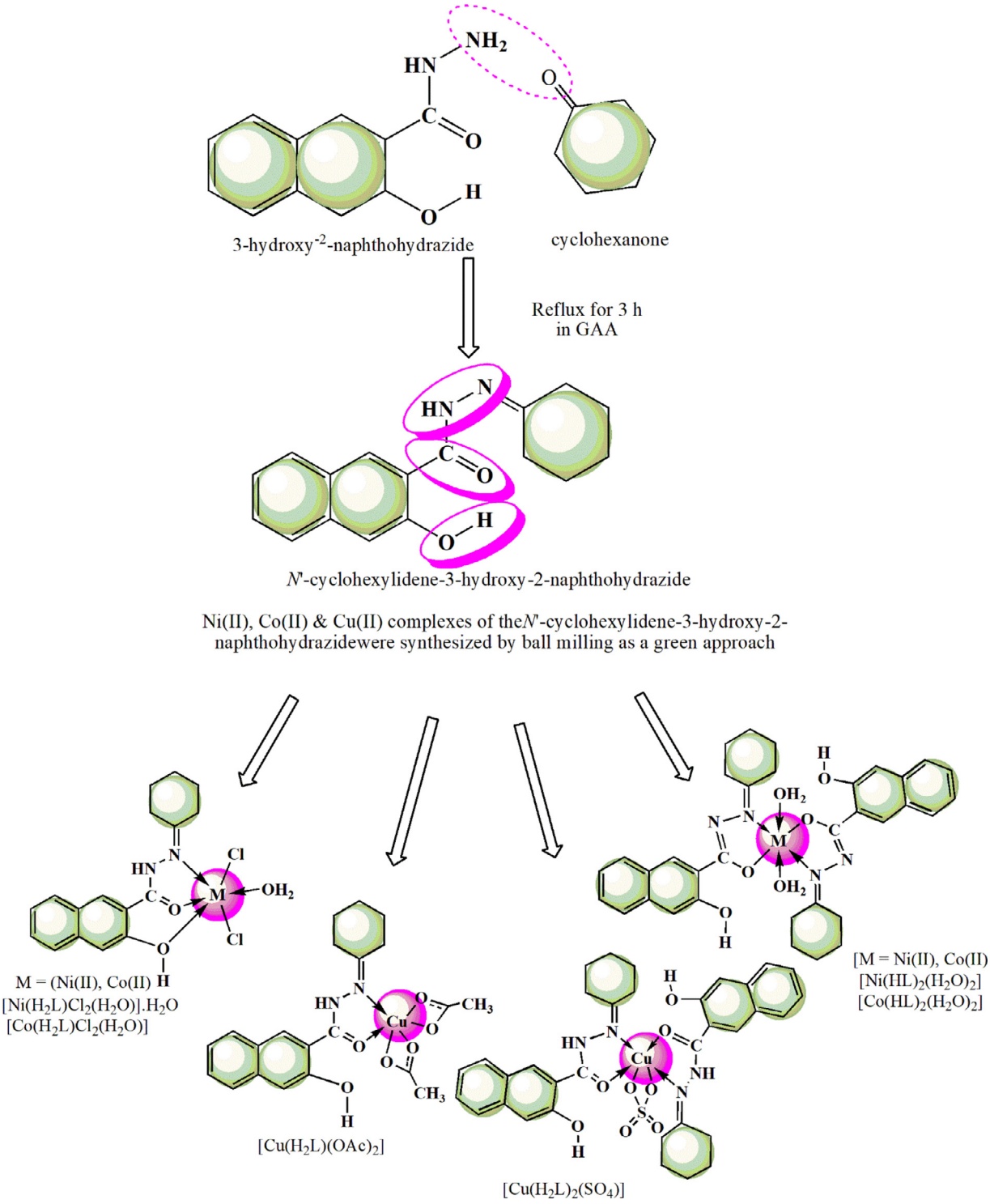

Scheme 1. The suggested products for performed reactions concerning ligand preparation and its metal complexes.

after characterization its was used to isolate Cu(II) and Ni(II) complexes [7]. Green synthesis of 4- and 6-coordination number from Pd(II), Ni(II) and Cu(II)-Schiff base complexes, was executed. Antimicrobial, antioxidant or antitumor activity was investigated for all synthesizes and most of them exhibited promising results [8]. Polymeric metal ion complex was investigated as a catalyst towards the decomposition of H_2O_2 [9]. Cu(II), Ni(II) and Co(II)-Schiff base complexes were prepared and characterized, then used as a catalyst for cyclohexane-oxidation by using hydrogen peroxide [10]. New Co(II), Ni(II) and Cu(II)-hydrazide complexes were prepared and exhibited antitumor activity [11]. In addition, Zn(II) and Cd(II) complexes were synthesized from new Schiff base derivative and intensive theoretical studies were executed [12]. It is worthy to mention that, the chemical synthesis caused many environmental problems in which the researchers tried to make their synthesis without hazardous. Consequently, the preparation in absence of solvent as a green protocol, is the aim already applied in many publications by using Ball-milling technique [[3], [6]]. A

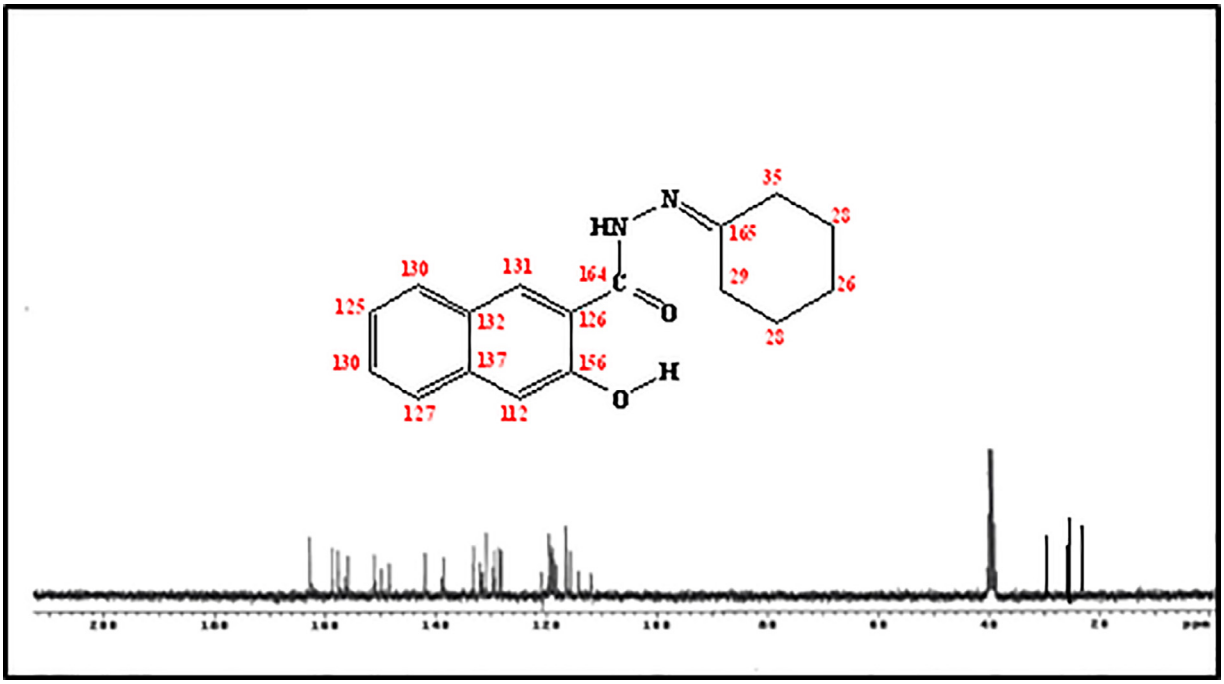

Fig. 1. ^{13}C NMR spectrum of H_2L in DMSO–d_6.

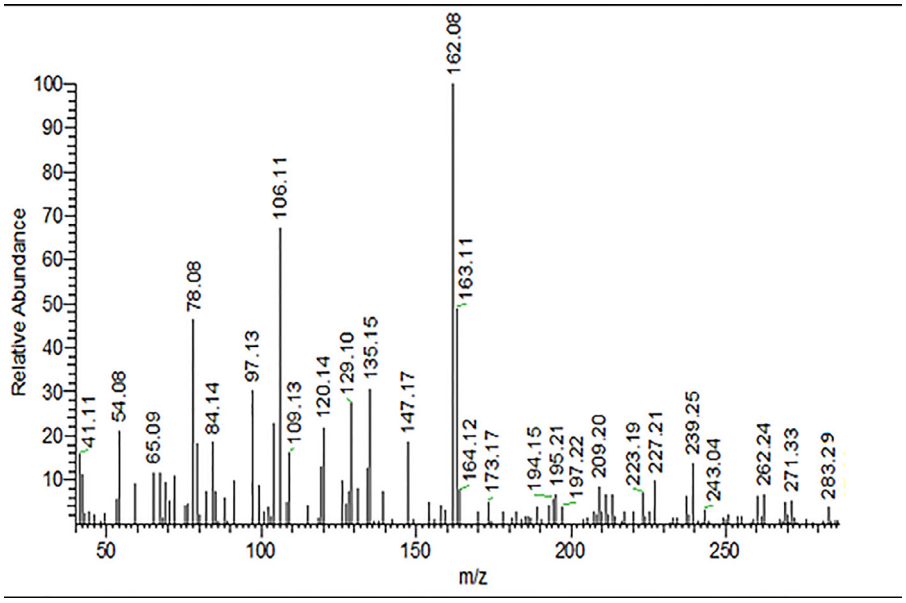

Fig. 2. Mass spectrum of H_2L.

perfect grinding for reactants (metal salt & ligand) by Ball-milling without solvent, leads to facile complexation that noticed firstly by changing the color away from initial compounds. The purity of complexes was evaluated by TLC after washing solid complexes many times by a suitable solvent [[8], [12], [13]]. Proceeding from all mentioned studies and in continuation for our work [13–19], we planned to synthesize new hydrazide derivative. Then and after characterizing the ligand, it was used to synthesize new complexes from $CuSO_4$, $Cu(OAc)_2$, $NiCl_2{\bullet}6H_2O$, $Ni(OAc)_2{\bullet}4H_2O$, $CoCl_2{\bullet}6H_2O$ and $Co(OAc)_2{\bullet}4H_2O$ salts. The preparation of complexes was carried out in absence of solvent as a green approach. This variation in conjugated anions (Cl^-, SO_4^{-2} &OAc^-), aims to differentiate the binding modes as well as the whole properties, accordingly. All complexes were investigated by available analytical, spectral and theoretical techniques. Conductometric study was executed in solution for selected complex. To predicate drug-like property as well as the inhibition activity of new compounds, pharmacokinetics and MOE-docking simulation, were performed, respectively. Finally, various *in-vitro* assays were executed for comparative evaluation and rank their activity.

2. Experimental steps

2.1. Reagents used for synthesis steps

3-Hydroxy-2-naphthoic acid hydrazide and cyclohexanone were obtained from Sigma & Aldrich as BDH and used to prepare hydrazide ligand. $CuSO_4$, $Cu(OAc)_2$, $NiCl_2{\cdot}6H_2O$, $Ni(OAc)_2{\cdot}4H_2O$,

Table 1
Important IR-spectral bands in H_2L and its metal complexes.

Compound; symbole	υ(OH) naphthoic	υ(NH)	υ(C = O)	υ(C = N)	υ(C = N*)	υ(C–O) naphthoic	υ(C–O) enolic	υ(M-O)	υ(M-N)
1)H_2L	3274	3142	1644	1624	–	1271	–	–	–
2)[Cu$(H_2L)_2(SO_4)$];Cu(II)- Bis(H_2L)	3432	3266	1636	1607	–	1272	–	532	423
3)[Cu$(H_2L)(OAc)_2$];**Cu(II)-H_2L**	3560	3270	1633	1606	–	1272	–	518	420
4)[Ni$(H_2L)Cl_2(H_2O)$].H_2O; **Ni(II)-H_2L**	3245	3150	1634	1608	–	1273	–	530	420
5)[Co$(H_2L)Cl_2(H_2O)$]; **Co(II)-H_2L**	3243	3149	1638	1606	–	1273	–	525	410
6)[Ni$(HL)_2(H_2O)_2$]; **Ni(II)-Bis(HL)**	3426	–	–	1596	1639	1244	1168	523	420
7)[Co$(HL)_2(H_2O)_2$]; **Co(II)-Bis(HL)**	3427	–	–	1593	1636	1242	1157	522	410

Table 2
Magnetic moments, electronic transitions and ligand field parameters.

Compound	$\mu_{eff.}$ (B.M.)	Band position (cm^{-1})	D_q (cm^{-1})	B (cm^{-1})	β	υ_2/υ_1
[Ni$(H_2L)Cl_2(H_2O)$].H_2O	2.98	15,106; 25,641	937	852	0.88	1.63
[Ni$(HL)_2(H_2O)_2$]	3.23	16,667; 26,666	1066	761	0.73	1.75
[Co$(H_2L)Cl_2(H_2O)$]	5.12	14,550; 18,316	793	835	0.86	2.15
[Co$(HL)_2(H_2O)_2$]	4.91	14,814; 17,391	767	767	0.79	2.15
[Cu$(H_2L)_2(SO_4)$]	1.97	17,391	–	–	–	–
[Cu$(H_2L)(OAc)_2$]	2.01	16,000	–	–	–	–

$CoCl_2{\cdot}6H_2O$ and $Co(OAc)_2{\cdot}4H_2O$ were the salts used to prepare series of complexes. Glacial acetic acid, ethanol, DMSO (Dimethyl sulfoxide) and DMF (Dimethylformamide) were extra-pure and used without preliminary treatments. These former chemicals were purchased from Merck.

2.2. Synthesis stage

2.2.1. Synthesis of hydrazide ligand

Firstly the ligand was prepared from reaction of 3–hydroxy-2-naphthoic acid hydrazide (0.01 mol; 3.06 g) and cyclohexanone (0.01 mol; 1.04 g), in 20 ml glacial acetic acid. This mixture was refluxed and stirred for 3 h to complete aimed condensation reaction. The solid precipitate was filtered off then recrystallized by using ethanol and dried over $CaCl_2$ in vacuum desiccators (Scheme 1). Yellow crystals obtained, M.P. 235 °C; Analytical data ($C_{17}H_{18}O_2N_2$), C (%): 72.12 (Calcd.72.33), H(%): 6.48 (Calcd. 6.39). IR (KBr-disk) (Fig. 1S); 1644, 1624, 3142 and 1271 cm^{-1} for $\upsilon(C = O)$, $\upsilon(C = N)$, υ(NH) and $\upsilon(C{-}O)_{naphthoic}$, respectively. Also, ^{1}H NMR spectrum (DMSO–d_6, Fig. 2S) of the ligand exhibited the following signals; δ (ppm): 1.52–1.57 (m, 6H, -$CH_2CH_2CH_2$- of cyclohexanone); 2.37–2.43 (m, 4H, 2 -CH_2- ortho-position for $C = N$ in cyclohexanone); 7.32–7.95 (m, 5H, Ar-H); 8.57 (s, 1H, Ar-H); 11.27 (s, 1H, NH), 11.58 (s, 1H, OH). ^{13}C NMR spectral data were typed on the graph (Fig. 1) for simplicity. Mass spectrum (Fig. 2); *m/z* (ppm) = 283.29 (5.22%) assigns to [M^++1] for $C_{17}H_{18}O_2N_2$ (M.W. = 282.34). These analyses confirm the formula suggested for the ligand which abbreviated by H_2L in this article based on presence of two labile hydrogen atoms in OH and NH–$C = O$ groups, which may be ionized.

2.2.2. Synthesis of complexes

Equi-molar amounts from the ligand (2 mmol, 0.565 g) and each metal salt as follow; $CuSO_4$ (0.319 g), $Cu(OAc)_2$ (0.245 g), $NiCl_2{\cdot}6H_2O$ (0.475 g), $Ni(OAc)_2{\cdot}4H_2O$ (0.498 g), $CoCl_2{\cdot}6H_2O$ (0.476 g) and $Co(OAc)_2{\cdot}4H_2O$ (0.498 g) were mixed in Ball-milling and grinded till complete complexation. The purity of products was tested by TLC after washing many times by EtOH. This test was carried out after dissolving the ligand in EtOH and each complex in DMSO solvent. A spot was taken from each solution and put in a thin layer chromatography plate. Then the plate was put in the mobile phase (petroleum ether: ethyl acetate, 3:1). The complex spot migrated over the plate by different retention factor (RF) than the ligand, which indicates its purity. Such facile synthesis step was applied to produce the aimed complexes which then analyzed to know their chemical formulae.

Analytical data; Found (Calcd.)

Green solid complex (M. P. 280 °C); [Cu$(H_2L)_2(SO_4)$] ($CuC_{34}H_{36}O_8N_4S$, M.W.= 724.28); C(%) 56.52 (56.38); H(%) 5.09 (5.01); Cu(%) 8.84 (8.77); SO_4 (%) 13.30 (13.26). Green solid complex (M. P. 284 °C); [Cu$(H_2L)(OAc)_2$] ($CuC_{22}H_{27}O_6N_2$, M.W.= 479.01); C(%) 54.52 (55.16); H(%) 5.06 (5.68); Cu(%) 13.78(13.27). Green solid complex (M. P.>300 °C); [Ni$(H_2L)Cl_2(H_2O)$].H_2O ($NiC_{17}H_{22}O_4\ N_2Cl_2$, M.W.=447.97); C(%) 46.19 (45.58); H(%) 5.04 (4.95); Ni(%) 13.21 (13.11); Cl(%) 16.00 (15.83). Green solid complex (M. P. >300 °C); [Ni$(HL)_2(H_2O)_2$] ($NiC_{34}H_{38}O_6N_4$, M.W.= 657.38); C(%) 62.05(62.12); H(%) 5.72(5.83); Ni(%) 8.91(8.93). Brown solid complex (M. P.>300 °C); [Co$(H_2L)Cl_2(H_2O)$] ($CoC_{17}H_{20}O_3N_2Cl_2$, M.W.= 430.20); C(%) 47.59(47.46); H(%) 4.53(4.69); Co(%) 13.64(13.70); Cl(%) 16.40(16.48). Brawn solid complex (M. P. >300 °C); [Co$(HL)_2(H_2O)_2$] ($CoC_{34}H_{38}O_6N_4$, M.W.= 657.62); C(%) 62.75(62.09); H(%) 5.94(5.82); Co(%) 8.96(8.96)

2.3. Analytical techniques

The complexes were synthesized using ball milling. A container filled with 10 cm3 stainless steel, double-walled tube, and two stainless steel balls make up the Retsch MM2000 swing mill (12 mm diameter and 7 g weight). At room temperature, ball-milling was performed at 20,225 Hz, 100 Hz, for 1/2 hour. Perkin-Elmer 2400 CHN Elemental Analyzer was used to extract the percentages of elements (carbon, hydrogen, and nitrogen). Also, complexometric titration and gravimetric analysis were used to determine the metal content and conjugated anion (Cl^- or $SO_4{}^{-2}$) [14]. JENWAY model 4070 Conductance Bridge was used to record conductance measurements (in DMSO). The IR and NMR spectra were obtained from JASCO FT-IR-4100 spectrophotometer (400–4000cm^{-1}) and Burker (500 MHz). Unicam spectrophotometer was used to scan the dissolved samples (in DMSO) to obtain UV–Vis spectra, while the balance of Johnson Matthey was used to determine magnetic susceptibility. The mass spectral analysis was performed at 70 eV using an AEIMS 30 mass spectrometer with a heating rate of 40 °C/min and a mass/charge scanning range of 50–1000. At 25 °C, EPR spectra were obtained using Jeol JES-RE1X spectrometer (9.435 GHz) and DPPH as a reference. Shimadzu Thermogravimetric Analyzer was used to derive TGA/DTG curves (20–900 °C). Under nitrogen, the heating rate was 10 °C min^{-1}. On an X-ray diffractometer (GNR, APD2000PRO, Italy) with a graphite monochromator, XRD patterns ($10^\circ < 2\theta < 90^\circ$ rang) were

Table 3
ESR Data of the Copper (II) Complexes at Room Temperature.

Complex	$g_{\|\|}$	$g_{\perp}$	$A_{\|\|}$ *(cm^{-1})	G	$g_{\|\|}$/ $A_{\|\|}$	α^2	β^2	Symm.
$[Cu(H_2L)_2(SO_4)]$	2.25	2.07	159	3.5	141	0.75	0.86	O_h
$[Cu(H_2L)(OAc)_2]$	2.21	2.06	162	6.3	136	0.72	0.63	O_h

$A_{\|\|}{}^{*} = A_{\|\|}$ x 10^{-4}.

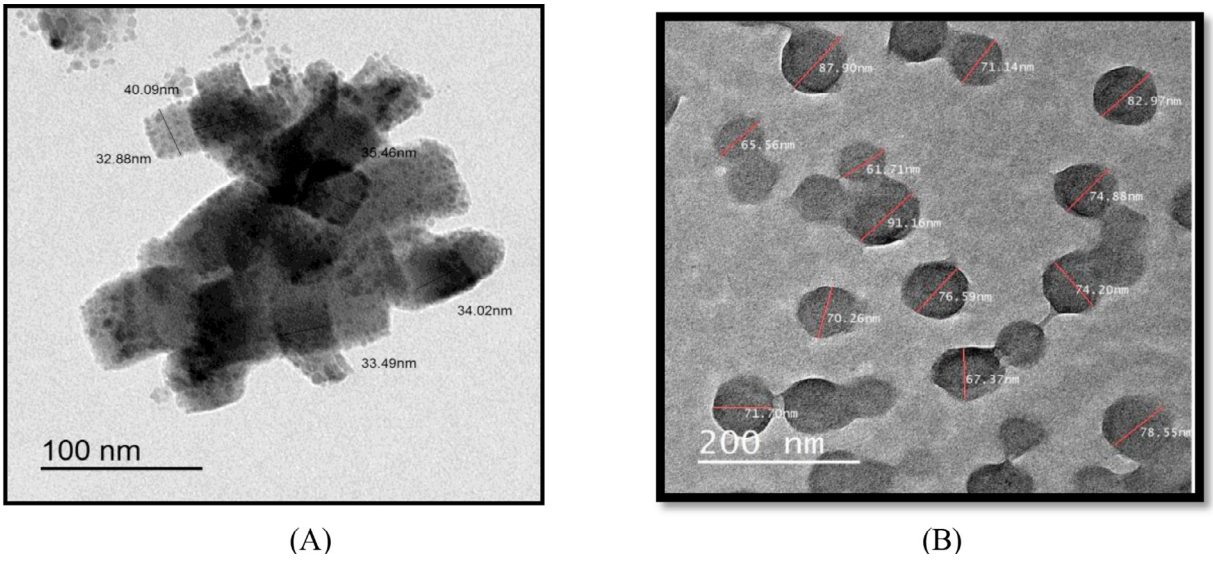

Fig. 3. TEM of (A) $[Cu(H_2L)(OAc)_2]$ and (B) $[Cu(H_2L)_2(SO_4)]$ complexes.

obtained. Using Cu/Kα1 radiation, the scanning rate is 0.03° min^{-1}. Joel JSM-6390 equipment was used to view SEM images. X-Ray Energy Dispersive Spectroscopy

2.4. Preparations for conductometry

The ligand (H_2L) solution (10^{-3} M) was prepared by dissolving 0.0282 g in 5% DMF/MeOH mixture. Also, $Cu(OAc)_2$ solution (10^{-4} M), was prepared by dissolving 0.0245 g in the same mixture, 5% DMF/MeOH. Titrate 20 mL from Co(II) solution with ligand solution (in burette). Sequentially, after adding each 0.2 mL ligand, measure the conductivity value by using HANNA, H1 8819 N type (cell constant = 1) (at 25 °C). Notice; the conductometer was attached with digital thermometer and ultra-thermostat (Kottermann 4130).

2.5. Molecular modeling

Materials Studio package was applied through DMOL3 program [20], to optimize all structural forms and estimate the quantum parameters. Schiff base ligand and its complexes were structurally configured by using DFT through exchange-correlation functional method of Becke3–Lee–Yang–Parr (B3LYP) [21]. DNP basis set [22] of GGA in PBEPBE functionals [23] as exchange-correlation function, was the suitable one for energy minimization that proceeded for optimization. Furthermore, the maps of electrostatic potential were performed over optimized structures by using B3LYP/6–31 G (d) level.

2.6. Biological simulation studies

2.6.1. Pharmacophore

The interaction models were obtained for most new compounds with two functional DNA-proteins (6va5 & 1kzy)(Scheme 1S). These proteins were PDB co-crystal forms which treated with each compound after uploading on Pharmit link (http://pharmit.csb.edu) [24]. Each interaction profile was achieved according to ligand-based type and also the binding types such as, H-bond acceptor (H-acc), H-bond donor (H-don), basic (H-bas) and acidic (H-acid), were counted. After that we started running for search in MolPort drug-library which updated at 2020–oct-14, 21:12:10 and includes 110,309,969 conformers for 7666,850 molecules [25]. This Pharmacophore search aims to extract analogues drugs which already certified to confirm therapeutic feature of tested compound.

2.6.2. Molecular docking

Molecular Operating Environmental module (MOE, ver. 2018) [26], is the program certified from drug industry which caused a revolution in the field of drug designing. This docking process simulates the behavior inside infected cell and put a respectable answers for many questions. What happened inside the cell after treatment using the suggest drug what is the interaction features with amino acids base-pairs, all of these question could be answered. Two selected DNA-proteins (6va5 & 1kzy) in their co-crystal forms were obtained from Protein Database [27] for docking purpose with new compounds. Such *in-silico* assay could being started after doing several steps to orient both docking sides as the suggested inhibitor (compound) and targeted protein. Inhibitor under test must face energy minimization, render for atomic charges and identifying potential energy value. Then open new database and save the oriented structure as MDB format to be ready for docking.

On the other hand, each protein must also being oriented through many steps to be suitable for docking. Firstly remove the water molecules attached with co-crystal, then put H-atoms over selected receptors and dummies in agreement to MMFF-force field [27]. Connect receptors, fix potential energy and then search for allosteric binding sites over protein helix and clarified the dummies. Therefore, select MDB file and start the docking process which covers trials over 30 poses to reach the most stable one. These poses

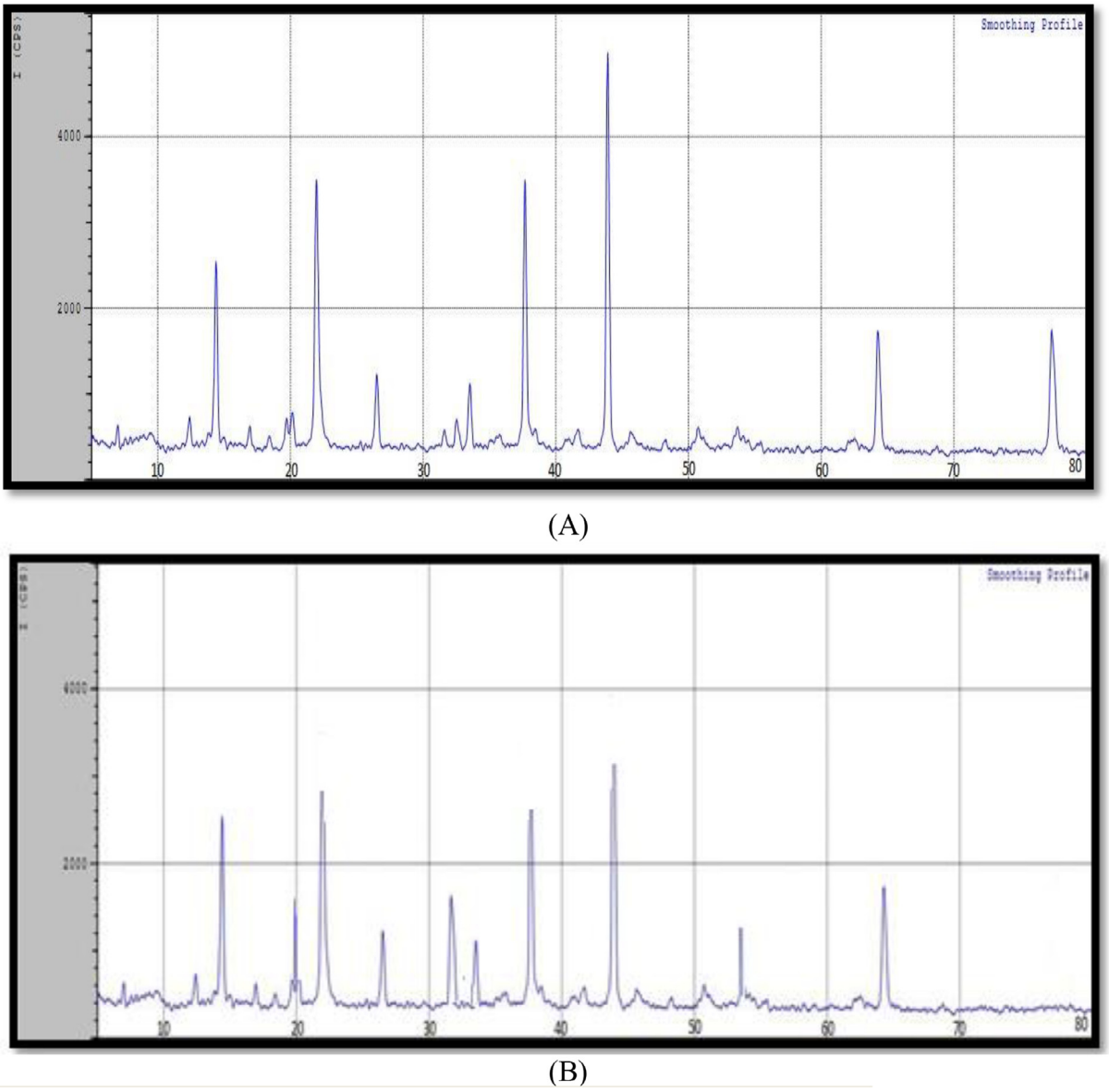

Fig. 4. XRD of (A) $[Cu(H_2L)(OAc)_2]$ and (B) $[Cu(H_2L)_2(SO_4)]$ complexes.

were controlled by London dG-scoring function which advanced twice times by triangle-matcher [28]. Some of these poses are completely unacceptable due to they yielded from un-preferable clash between the compound and protein pockets. Each docking process produced interaction parameters, docking patterns and interaction molecular surfaces which they used to order the inhibition efficiency of tested compounds. This according to H-bond length which must agree with Van der Waals radii (< 3.5 Å) as well as the docking score values which estimated from this relation; docking Score (force fields)= - ((receptor interaction energy / ligand) + ligand internal energy) [28].

2.7. Biological screening

2.7.1. Antimicrobial investigation

Agar well diffusion technique was applied *in-vitro* screening that detailed in the supplementary file (Scheme 2S) [29]. Inhibition behavior of all synthesizes was examined towards *Staphylococcus aureus* (*G*+ve), *Escherichia coli* (G-ve) and *Candida albicans* (fungus). 100 µg/mL were the stock solution concentration that prepared from each tested compound in DMSO solvent. Finally, after implementing the steps presented (Scheme 2S), inhibition zones were measured. Inhibition activity index (%) was estimated according to reference drug (antibiotic ampicillin or antifungal Colitrimazole) by using this equation;%= (diameter of inhibition zone under influence of tested compound / diameter of inhibition zone under influence of standard) × 100

2.7.2. Anti-oxidant and antitumor activity

ABTS-assay was applied to test antioxidant efficiency of all new compounds which typed briefly in Scheme 3S [30]. The reagent used [2, 2-azinobis-(3-ethylbenzthiazoline- 6-sulphonic acid), ABTS] in this study and the reference drug (L-ascorbic acid) were purchased from Sigma & Aldrich. The mixtures prepared must be shaken carefully, centrifuged and finally filtrated off. The resulting greenish-blue color intensity of ABTS-radical was measured ($A_{control}$) at λ=734 nm. Then the absorbance (A_{test}) was monitored after addition of 2 mM from the tested compound (50μL) which prepared in spectroscopic grade solvent, MeOH/buffer (1:1; v/v). The decay of color intensity is a measur-

Table 4
Formation constants and Gibbs free energies of formation for 2:1 (M/L) Co(II)-(H_2L) complex in DMF/Methanol at 290.15 K.

Λ_{obs} ($cm^2.Ohm^{-1}$)	[L]	(Λ_{obs}-Λ_{ML}) [L]	(Λ_M-Λ_{obs})	K_f	G_f	ΔG_f (k J/mol)
92.44	5.70E-05	2.559E-05	4.970	194,178	−29,779	−29.779
93.20	6.55E-05	7.962E-05	4.208	52,790	−26,594	−26.594
93.75	7.44E-05	0.000130669	3.658	27,980	−25,041	−25.041
94.83	9.11E-05	0.000258183	2.580	9993	−22,523	−22.523
95.24	9.92E-05	0.000322866	2.163	6697	−21,544	−21.544
96.17	0.000139	0.000577112	1.237	2142	−18,756	−18.756
96.92	0.000176	0.000857531	0.480	559	−15,470	−15.470
96.93	0.000189	0.000924489	0.478	515	−15,268	−15.270

Λ_M = 97.4 $cm^2.Ohm^{-1}$, Λ_{ML} = 91.98 $cm^2.Ohm^{-1}$.

able for scavenging activity for free radicals and the activity index could be determined by this relation; [$A_{(control)}$- $A_{(test)}$/$A_{(control)}$] × 100. Notice; ascorbic acid (vitamin c) was the positive control and the blank solution was methanol/phosphate buffer (1:1) without ABTS and tested compound.

The antitumor screening was performed for all compounds versus liver carcinoma cell line (HepG2) according to MTT method [31] as schematically displayed in the supplementary file (Scheme 4S). The reagents used as well as the tumor cell line were available from holding company for biological reagents and vaccines (VACSERA). For comparison, 5-fluorouracil was the positive control used and cell-viability percentage was estimated from this relation; (A_{570} of tested samples/A_{570} of untreated sample) × 100).

3. Results and discussion

3.1. General properties

Co(II), Ni(II) and Cu(II)-hydrazide complexes were prepared from variable anionic salts (Cl^-, SO_4^{-2} & OAc^-), to examine the impact of conjugated anion on the ligand coordination mode as well as the whole features. The analytical and spectral data verified variations in mode of coordination within the complexes, which also appeared by two different stoichiometry as 1:1 and 1:2 (M:L) molar ratio. The molar conductivity of complexes (1 mmol) were determined (in DMSO) and the values were 3.3–7.9 $Ohm^{-1}cm^2mol^{-1}$ range, which agree with non-electrolytic property [32]. This property may refer to the preferable coordination ability of SO_4^{-2} & OAc^- anions. While, the complexes prepared from chloride salts exhibited covalent and ionic presence of chloride ion, due to the high similarity between the two features (ionic & covalence) for this anion.

3.2. Mode of coordination

IR- spectral analysis was carried out for the free ligand and its complexes (Fig. 1S) to remark the changes on significant vibrational bands after complexation. Table 1 summarizes important vibrations for functional groups, to extract the mode of bonding within Co(II), Ni(II) and Cu(II) complexes. $\upsilon(C=O)$, $\upsilon(C=N)$, υ(NH) and υ(C–O)$_{naphthoic}$ vibrations were appeared at 1644, 1624, 3142 and 1271 cm^{-1}, respectively [33] in H_2L ligand spectrum. The shifts observed for these bands suggest either neutral or monobasic feature with bidentate or tridentate binding mode. While, the coordination number was elevated due to contribution of auxiliary ligands (secondary) as water or anion molecules.

In [$Cu(H_2L)_2(SO_4)$] and [$Cu(H_2L)(OAc)_2$] complexes spectra, H_2L binds as a neutral bidentate ligand *via* carbonyl oxygen and azomethine nitrogen. This is due to lower shift of $\upsilon(C=O)$ and $\upsilon(C=N)$ vibrations in their spectra. Vibrational band of υ(NH) kept more or less un-shifted due to its ruling out from coordination. While, non-coordinating OH group pushed shift in $\upsilon(OH)_{naphthoic}$ band to higher wavenumber [34]. Acetate or sulfate group revealed two bands at 1539, 1420 and 1444, 1250 cm^{-1} which can be assigned to asymmetric and symmetric vibrations, respectively. The gap between υ_{as}(OAc) and υ_s(OAc) (Δ = 95 cm^{-1}) indicates the bidentate nature of the group.

A neutral tridentate binding mode of H_2L ligand was suggested in [$Ni(H_2L)Cl_2(H_2O)].H_2O$ and [$Co(H_2L)Cl_2(H_2O)$] complexes, according to noticeable shifts in definite spectral bands. Azomethine nitrogen, carbonyl oxygen and $(OH)_{naphthoic}$ were the coordinating centers with the two metal ions. This is based on lower shifted appearance of their vibrational bands. IR spectra of [$Ni(HL)_2(H_2O)_2$] and [$Co(HL)_2(H_2O)_2$] complexes, point to presence of mononegative bidentate ligand. The ligand coordinates *via* azomethine nitrogen and enolized carbonyl oxygen (=C–O^-) after ionization. This suggestion is based on disappearance of both $\upsilon(C=O)$ and υ(NH) vibrations with instantaneous appearance of $\upsilon(C=N^*)$ and υ(C–O) vibrations [35] beside the lower shift of $\upsilon(C=N)$ band.

Generally, the spectra of all complexes showed new bands at lower wavenumber region which attributed to υ(M-O) and υ(M-N) vibrations. Also, chelation yields five membered rings with central metal atom and the coordination number was generally elevated by secondary ligands (anion or H_2O) till six. $\rho_r(H_2O)$ and $\rho_w(H_2O)$ vibrations were observed in the spectra of Co(II) and Ni(II) complexes, at 860–871 and 761–783 cm^{-1} region, respectively.

3.3. Electronic transitions and magnetic moments

UV–Vis spectroscopy is considered the most significant technique used to monitor electronic transitions inside chemical compounds particularly transition metal ion complexes. This specification is referring to the changes happened in d-orbitals under influence of ligand filed (Table 2). Such changes offer interesting transitions parallel to geometry of complexes and electronic configuration of central metal [36]. UV–Vis spectra of [$Co(H_2L)Cl_2(H_2O)$] and [$Co(HL)_2(H_2O)_2$] complexes (Fig. 3S) showed two bands at 14,550, 14,814 and 17,391, 18,316 cm^{-1} respectively, which correspond respectively to $^4T_{1g} \rightarrow {}^4A_{2g}(F)$ and $^4T_{1g} \rightarrow {}^4T_{1g}(P)$ transitions, in octahedral arrangement [37]. The ligand field splitting energy (D_q), Racah parameters (B) and nephelauetic ratio (β) were estimated (Table 2) and matched with that reported for octahedral Co(II) complexes [37]. The first transition which is always out of scanning range, was also calculated (υ_1; 6767 &6815 cm^{-1}) [36]. Furthermore, their magnetic moment values (5.12 & 4.91 B.M.) add another evidence for high-spin octahedral geometry.

UV–Vis spectra of [$Ni(H_2L)Cl_2(H_2O)].H_2O$ and [$Ni(HL)_2(H_2O)_2$] complexes showed two bands at 15,106, 16,667 and 25,641, 26,666 cm^{-1} regions assignable to $^3A_{2g} \rightarrow {}^3T_{1g}(F)$ and $^3A_{2g} \rightarrow {}^3T_{1g}(P)$ transitions, respectively. Their ligand field parameters (D_q, B & β) were calculated and found within the normal range of octahedral centered by Ni(II) ion [14]. The value of υ_1 (9267 &10,615 cm^{-1}, re-

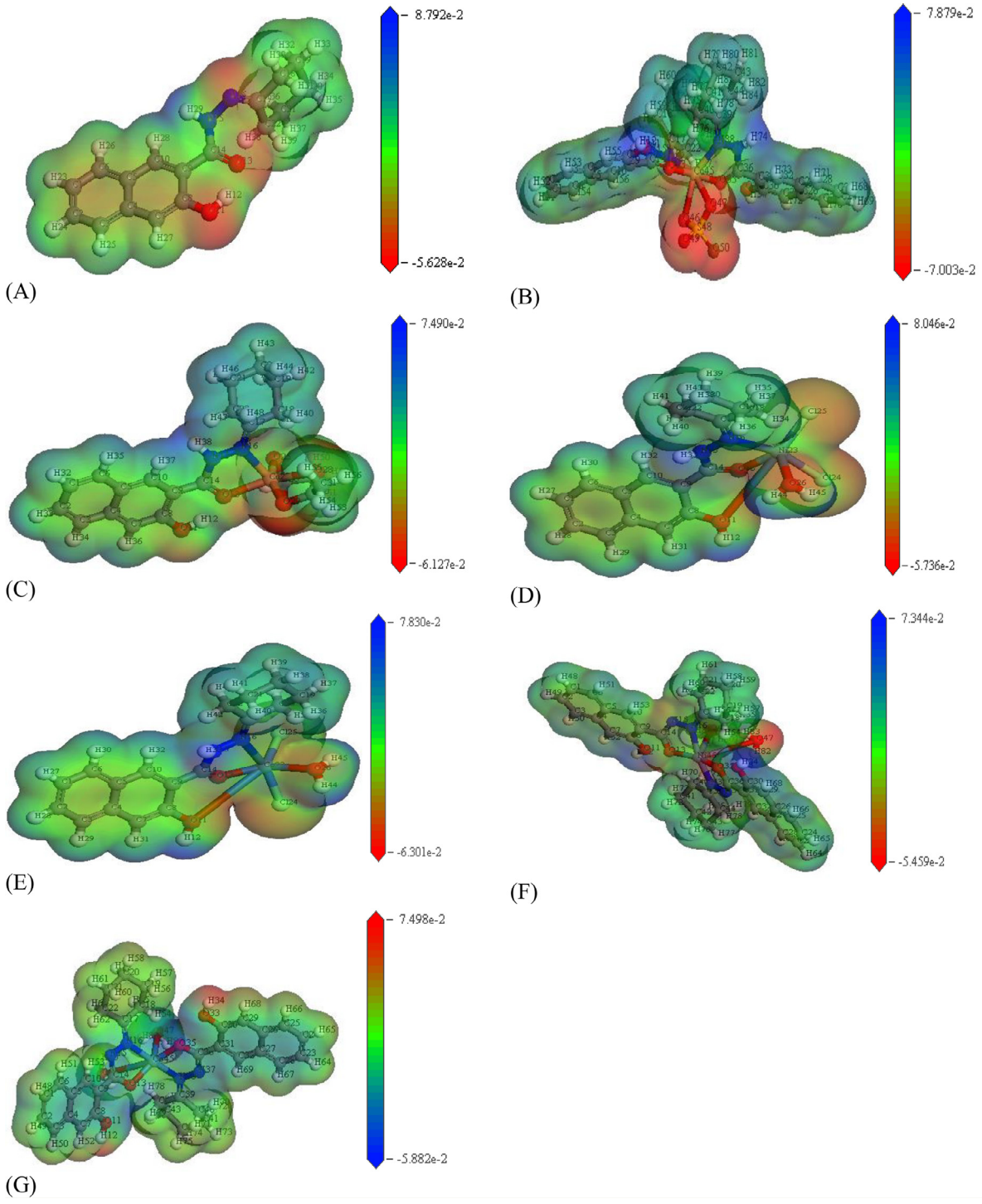

Fig. 5. MEP of (A)H_2L, (B)[$Cu(H_2L)_2(SO_4)$], (C)[$Cu(H_2L)(OAc)_2$] (D)[$Ni(H_2L)Cl_2(H_2O)$].H_2O, (E)[$Co(H_2L)Cl_2$ (H_2O)], (F) [$Ni(HL)_2(H_2O)_2$] and (G) [$Co(HL)_2(H_2O)_2$].

spectively) was also calculate. The magnetic moment values were 2.98 and 3.23 BM, respectively, for outer orbital octahedral arrangement. As known, no significant information could be estimated from either the magnetic moment or the electronic transitions in Cu(II) complexes, to discriminate its structural forms. UV–Vis spectra of [$Cu(H_2L)_2(SO_4)$] and [$Cu(H_2L)(OAc)_2$] complexes (Fig. 3S) showed characteristic bands at 17,391 and 16,000 cm^{-1} assigned to $^2E_g \rightarrow {}^2T_2g$ transition, in octahedral configuration which must be distorted according to Jahn-Teller effect [38].

3.4. ESR-spectra

Electron Spin Resonance analysis is an essential tool for paramagnetic compounds and was executed for the two Cu(II) complexes, to estimate Hamiltonian factors (g & f) [39] and to confirm their octahedral configuration (Fig. 4S). Hyperfine splitting ($S = 1/2$, $I = 3/2$) that depends on resolving microstates in D_{4h} symmetry ($m_l = 3/2, 1/2, -3/2$ &$-1/2$), was fairly noticed in the two spectra. Consequently, field vector (g) can be calculated while anisotropic parameters couldn't estimate except the parallel one ($A_{//}$), due to

smooth feature of hyperfine (Table 3). Hamiltonian parameters calculated (Table 3) agree perfectly with that reported for octahedral configuration with ^2A_1g (d_X^2-$_Y^2$) ground term. Due to complex formation, g-vectors ($g_{//}>g_{\perp}>2.0023$) were shifted from that of free electron (2.0023) according to spin-orbital coupling ($\lambda=-828$). The interaction factor (G) was estimated to evaluate the degree of interaction between centers in adjacent particles and obtained from this relation; $G = (g_{//}-2.0023)/(g_{\perp}-2.0023)$.

With respect to $[Cu(H_2L)_2(SO_4)]$ complex, the value of $G = 3.5$, closes to normal value (4) which reflects insignificant interaction between copper centers in neighboring particles. While, the second complex the value of $G = 6.3$, reflects the absence of any interaction between copper centers [40]. Furthermore, tetrahedral distortion index ($f = g_{//}/A_{//}$) was calculated according to parallel anisotropic parameter ($A_{//}$ x10^{-4}). The two values were higher than 135 which coincide with octahedral geometry values. Moreover, the in-plane bonding factors as σ-bonding (α^2) and π-bonding (β^2), were also estimated from these relations; $\alpha^2=(A_{//}/0.036)+(g_{//}-2.0023)+ 3/7(g_{\perp} - 2.0023)+0.04$ and $\beta^2 = (g_{//} -2.0023)E/(-8\lambda\alpha^2)$ [41]. The two values were appeared close to unity, which indicates the ionic property of new M-L bonds.

3.5. SEM, TEM and XRD analyses

To investigate topography of surface for two selected complexes (i. e., Fig. 5S), SEM technique photographs the powdered samples, to identify morphology, particle shape, crystallinity and chemical composition [42]. Energetically stimulated electrons were accelerated to interact solid surfaces and then generate various signals to pick up the targeted 2-D images (Fig. 5S). The micrographs displayed the particles with irregular broken ice rock-like which accompanied with fine micrometer-sized grains that randomly distributed over such ice rock structures [42].

TEM technique was implemented by using beam of electrons to penetrate solid specimens of $[Cu(H_2L)_2(SO_4)]$ and $[Cu(H_2L)(OAc)_2]$ complexes (Fig. 3). This enables to capture fine-details in solid samples as the high homogeneity of $[Cu(H_2CHNH)_2(SO_4)]$ complex surface with particulate sizes of 30 - 40 nm range. While, the surface of second complex appeared with high aggregation for tiny particles till reach to size range from 60 to 90 nm [42].

XRD patterns of $[Cu(H_2L)(OAc)_2]$ and $[Cu(H_2L)_2(SO_4)]$ complexes (i.e.) were obtained to estimate the features of lattice dynamic (Fig. 4). This was carried out by using FWHM method [43] due to nano-crystallinity nature appeared in patterns. Regarding the pattern of $[Cu(H_2L)_2(SO_4)]$ complex, 2θ, D-spacing (Å), FWHM (β) and intensity (I) were calculated [44] to be 21.94°, 4.048, 0.23 and 530, respectively. In addition, the particulate size S (nm) is found to be 64.14 nm. While and regarding $[Cu(H_2L)(OAc)_2]$ complex pattern, 2θ, D-spacing (Å), FWHM (β) and intensity (I) were calculated [45] to be 21.95, 2.493, 0.222 and 311, respectively. In addition, the particulate size S (nm) is found to be 66.45 nm.

Unit-cell for crystal packing system of the two Cu(II) complexes, was demonstrated by using VESTA package [46] (Fig. 6S) to recognize the type of atomic arrangement inside the lattice. The style of simple repeated unit for the two complexes seems to be face-centered cubic unit. This is based on presence of lattice point (metal) in corners of cubic-cell as well as other centered in each face. This property was appeared perfect with $[Cu(H_2L)(OAc)_2]$ unit-cell, while the other complex appeared with indefinite packing system.

3.6. Thermogravimetric analysis

TGA curve of $[Ni(H_2L)Cl_2(H_2O)].H_2O$ complex was obtained (Fig. 7S), to confirm presence of coordinating and hydrating water molecules. The plausible degradation behavior was detailed in Table 1S. The first step exhibited removal of hydrated water molecule below 100 °C by 4.1% weight loss. While the coordinating one was removed in the second step beside Cl_2 molecule at 234–347°C range by19.8% weight loss. The reaming part of coordinating ligand was degraded upon other two successive steps till 532 °C, the behavior in third step was schematically presented (Scheme 2). In which, the residual part was recorded and the weight percentage (16.6%) closes to NiO formula.

3.6.1. Thermo-kinetic parameters

As known, the thermogravimetric analysis stages are kinetically controlled and we could estimate kinetic and thermodynamic parameters. These parameters are essential to characterize thermal decomposition behavior along the applied temperature range. So, the decomposition rate which is a relation between k(T) and f(α) was as follow;

$$\frac{d\alpha}{dt} = k(T)f(\alpha) \quad (1)$$

In which, α is a fraction decompose at time t, f(α) is a conversion function and k(T) is a function dependent on temperature. These functions are of Arrhenius type (2).

$$K = A e^{-E*/RT} \quad (2)$$

In which, R is the gas constant (J $mol^{-1}k^{-1}$), then by using relation 2 as a function of relation 1, such relation could being obtained (3);

$$\frac{d\alpha}{dt} = \left(\frac{A}{\varphi e^{-E*/RT}}\right) f(\alpha) \quad (3)$$

In which, β is a linear heating rate (dT/dt), T_o is the starting temperature and $T = T_o + \beta_t$. As we know that, several decomposition processes have been exhibited first order reaction. Therefore, we assumed $n = 1$ and based on that the integration of previous equation leads to this relation;

$$\ln(1-\alpha) = -\frac{A}{\beta}\int_{T_0}^{T} Exp(-\frac{E_a}{RT})dT$$

Accordingly, it is possible to interpret the data obtained by integral method, to determine kinetics of degradation process (A&E_a). In the above equation, the integral in the right-hand side has no significant solutions and many approximations are commonly applied. Therefore, we used two variable methods as Coats-Redfern [47] and Horowitz-Metzger [48] that differ in resolving way, for assertion.

A Coats-Redfern

The relation used by Coats-Redfern is;

$$\ln[\frac{g(\alpha)}{T^2}] = \ln\left(\frac{AR}{\beta E}\right) - \frac{E}{RT}$$

In which, $g(\alpha) = 1\text{-}(1\text{-}\alpha)^{1\text{-}n}/1\text{-}n$ if $n \neq 1$ and $g(\alpha) = -\ln(1-\alpha)$ if $n = 1$,

R is the gas constant. The correlation coefficient (r) could being computed by using least square method under variable n values ($n = 0.33$, 0.50, 0.66 and $n = 1.00$), through a relation between $\ln[g(\alpha)/T^2]$ and 1/T for the complex as shown (Fig. 8S). The value (n) which gave best fit ($r \approx 1$) was selected as the order parameter for decomposition step under consideration. The kinetic parameters (E_a & A) were obtained from slope of straight line ($= E_a/R$) and the intercept which equal pre-exponential factor (A) and the data were displayed (Table 2S)

A Horowitz-Metzger Method

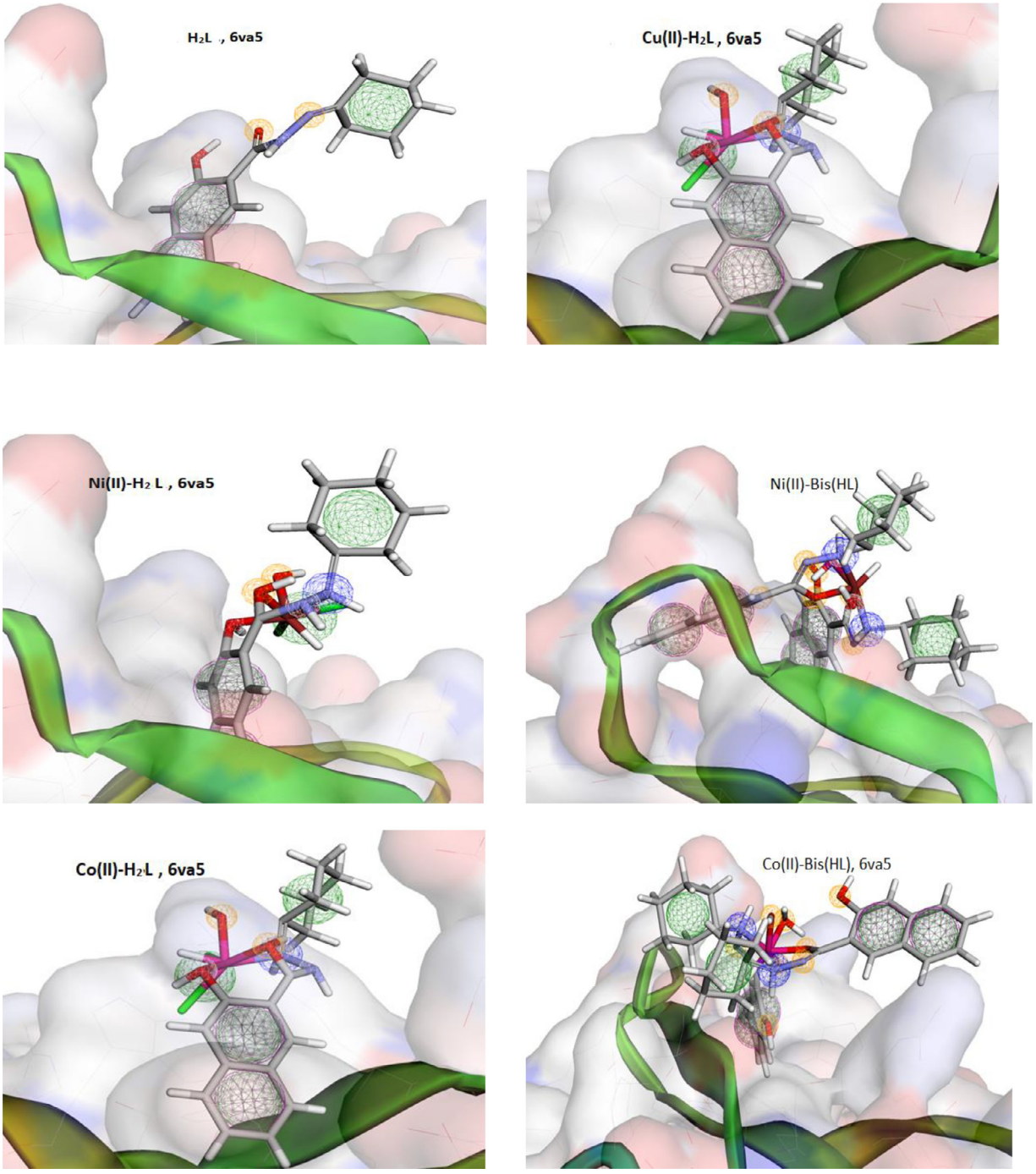

Fig. 6. Interaction profile for most synthesizes towards 6va5 protein.

These are the Horowitz-Metzger relations that used;

$$\ln[-\ln(1-\alpha)] = \frac{E_a^{\theta}}{RT_s^2} \text{ (n = 1)}$$

$$\ln\left[\frac{1-(1-\alpha)^{1-n}}{1-n}\right] = \ln(\frac{ART_s^2}{\beta}) - \frac{E_a}{RT_s} + \frac{E_a^{\theta}}{RT^2} \text{ (n} \neq 1)$$

In which, θ=*T*-Ts, Ts is the final stage temperature, T is the temperature consistent to the weight loss. The straight line obtained (Fig. 9S) from the relation between left hand side in the first equation (at $n = 1$ as applied) and θ, then the slope is E_a/RT_s^2 which used to estimate activation energy (Table 3S).

A Thermodynamic Parameters

After calculating kinetic parameters, ΔS, ΔH, A, E_a and ΔG were the thermodynamic indexes calculated from the following simple relations; $\Delta H = E - RT$, $\Delta S = R \ln h A / K_b T$ and $\Delta G = \Delta H - T\Delta S$ (Table 3S).

Finally, we could conclude the following remarks;

1) The kinetic parameters estimated showed better correlation at $n = 1$. 2) High activation energy values (E_a) reveal high stability of such complex [49]. 3) Negative sign of ΔS values, indicates more ordered activated complex than the incident reactants and the degradation process is nonspontaneous [50]. 4) Positive sign of ΔH values, indicates the endothermic characteristic of decomposition stages. 5) Positive sign of ΔG values, indicates the high free energy of degraded moiety than that of initial compound, which

Table 5
Interaction parameters within docking complexes towards selected DNA-proteins.

Compounds	Proteins	ligand	Receptor	Interaction	Distance(Å)	E(Kcal/mol)	S(energy score)
1) H_2L	6va5	O12	NH2 ARG 1490 (A)	H-acceptor	2.98	−3.6	−5.5133
	1kzy	O12 O12 O12	N SER 116 (A) N GLY 117 (A) NH1 ARG 282 (A)	H-acceptor H-acceptor H-acceptor	3.07 3.34 3.01	−3.3 −1.4 −1.9	−5.5948
2) Cu(II)- H_2L	6va5	O12 N15 C18	OE2 GLU 1598 (A) O ARG 1595 (A) CB GLU 1598 (A)	H-donor H-donor H-acceptor	2.59 3.11 3.82	−12.0 −4.6 −0.9	−5.3695
	1kzy	O11	O GLY 262 (B)	H-donor	3.21	−0.9	−5.7821
3) Ni(II)- H_2L	6va5	O17	OE2 GLU 1543 (A)	ionic	2.61	−7.6	−6.1810
	1kzy	O81 N21	OG SER 96 (B) OG SER 96 (B)	H-donor H-donor	3.15 3.27	−4.1 −1.5	−4.9872
4) Ni(II)- Bis(HL)	6va5	N38 O83 O83	OE2 GLU 1567 (A) OE2 GLU 1567 (A) OE1 GLU 1567 (A)	H-donor H-donor ionic	3.18 2.68 3.27	−10.6 −7.3 −7.0	−6.5028
	1kzy	O83 O83	OE2 GLU 258 (B) O GLY 262 (B)	H-donor H-donor	2.74 2.75	−12.1 −8.3	−6.9501
5) Co(II)- H_2L	6va5	–-	–-	–-	–-	–-	−5.6262
	1kzy	O18 N22	OE2 GLU 258 (A) O GLY 262 (A)	H-donor H-donor	2.78 3.06	−12.7 −2.9	−5.1828
6)Co(II)- Bis(HL)	6va5	O83 O83	OE1 GLU 1567 (A) OE1 GLU 1567 (A)	H-donor ionic	2.56 2.56	−13.9 −8.2	−6.7757
	1kzy	O83 O83	OD1 ASP 208 (B) OD1 ASP 208 (B)	H-donor ionic	2.60 2.60	−17.9 −7.8	−7.037

increased successfully from step to another. Also, due to increasing TΔS (-ve) from step to another which led to override ΔH values [50].

3.7. Conductometric measurements

3.7.1. Determination of complex stoichiometry

Although this research was focused on the coordination features in solid complexes, but the complex formed in solution offers interesting data may help in discussing their solid state. Conductometric measurements were done over freshly prepared solutions from $Co(OAc)_2{\cdot}4H_2O$ and hydrazide ligand (H_2L), to identify their binding behavior in solution state. Both of Co(II) ion and the ligand were mixed in DMF/methanol (5%) at 290.15 K, to estimate constants of association (K_A) and formation (K_f) beside their Gibbs free energy values (ΔG_A & ΔG_f). Both in absence and presence of H_2L ligand, the values of specific conductance (K_s) were determined with different Co(II) ion concentration. So and by using this equation; $\Lambda_m = (K_s - K_{solv})\ K_{cell} \times 1000/C$, the molar conductance (Λ_m) values were computed [51]. Where, K_s and K_{solv} are the solution and solvent specific conductance, respectively, while, K_{cell} is the cell constant (= 0.99) and C is the Co(II) concentration (M, mol/L). At infinite dilution, the limiting molar conductance (Λ_o), was obtained for Co(II) ion free from ligand (zero concentration) (Table 4S). A relation drawn between Λ_m and ligand /metal concentration [L/M] (Fig. 10S), leads to extract molar ratio for complex formed through intercept point between the two lines [51]. The formed L: M ratio was 2:1, which surprisingly matches that formed in the solid state.

3.7.2. Determination of association and formation constants

The association constant for the complex formed between Co(II) and H_2L ligand could being estimated from this equation; $K_A = {\Lambda_0}^2\ (\Lambda_0 - \Lambda_m) / 4{C_m}^2\ {}^2\gamma_{\pm}\ {\Lambda_m}^3 S_{(Z)}$ [52]. Where, C_m, $S_{(Z)}$ and $\gamma_{\pm}$are the molar concentration of Co(II) ion, Fuoss-shedlovsky factor (strong electrolytes = 1) and activity co-efficient, respectively. Moreover, Gibbs free energy of association (ΔG_A) can be obtained from the following relation; $\Delta G_A = -RT \ln K_A$, notice; R is the gas constant and T is the absolute temperature. Also, the formation constant for the complex formed (K_f) was estimated from the following equation; $K_f = \Lambda_m - \Lambda_{obs} / (\Lambda_{obs} - \Lambda_{ML})[L]$. Where, Λ_{obs} and Λ_{ML} are the molar conductance of solution during titration and for the complex formed, respectively. In addition, Gibbs free energy of formation (ΔG_f) can be obtained by the following relation; $\Delta G_f = -RT \ln K_f$. Thus, the constants either for association (K_A, ΔG_A) or formation constants (K_f and ΔG_f) were calculated and displayed (Table 4). The data suggested 1:2 molar ratio between Co(II) and ligand in 5% MDF/methanol solution. Such molar ratio agrees interestingly with that formed in solid state. This indicates its high stability without competition with other ratios expected with plentiful presence for ligand. Gibbs free energy values calculated appeared lower which points to the spontaneity of complexation reaction as usual.

3.8. Geometry optimization

3.8.1. Common properties

Materials Studio package was applied through DMOL3 program and DNP basis set [20], to optimize structural forms of Schiff base ligand and its Co(II), Ni(II) and Cu(II) complexes. The structural form yielded for H_2L ligand (Fig. 11S) showed Cis-orientation for N(16), O(11) and O(13) centers, which enables them for coordination with metal ions without twisting around the bonds or strain. Also, some bond angles in the ligand as C(8)-O(11)-H(12), C(8)-C(9)-C(14), O(13)-C(14)-N(15), N(15)-N(16)-C(17), suffer changes after complexation. The structural forms of complexes displayed bond angles centered by metal atom up to 90° and 180° which assigned to d^2sp^3 or sp^3d^2 hybridization in octahedral configuration. Also, the bond lengths of C(8)-O(11), O(11)-H(12), C(14)-O(13), N(15)-H(30), N(15)-N(16) and C(17)-H(31) appeared elongated than that in free ligand. This is a normal feature for each bond has an atom coordinating with central metal ion [53].

The HOMO and LUMO images (Fig. 12S) were demonstrated over the optimized forms, to discriminate electronic distribution in functional groups. The two orbitals appeared localized over naphthohydrazide moiety in free ligand. The appearance of these orbitals not changed strongly after complexation, the feature in all complexes are close to each other and their coverage is far from central metal surrounding [54].

3.8.2. Energy content of optimized forms

Energy minimization strategy is based on running the program till reach the most fitted stabilized configuration, in which the minimum energy content was obtained. Energy of, binding, formation, spin polarization, kinetic, electrostatic, exchange-correlation and the overall atomic, were computed beside the dipole moment and E_{HOMO} & E_{LUMO} (Table 5S, Fig. 13S). High stability was remarked with all complexes particularly $[Cu(H_2L)(OAc)_2]$ (3) and $[Ni(HL)_2(H_2O)_2]$ (6). This is based on reduced energy gaps (E_{LUMO}-E_{HOMO}) than that of free ligand as well as their lower energy contents. Consequently, the relationship between structure and activity, could being estimated based on dipole moment and frontier energy gaps ($\Delta = E_{LUMO} - E_{HOMO}$). According to dipole moment values, Ni(II)-Bis(HL), Co(II)-Bis(HL) and Cu(II)-Bis(H_2L) complexes,

reveal the lower values which is a promising feature in biological activity, because of high lipophilicity [55]. While, the energy gap has a direct relation with the activation energy values that affects in the complex-activity during catalytic applicability.

3.8.3. MEP maps

Molecular Electrostatic Potential maps (MEP) enable us to differentiate electron density over the functional groups (Fig. 5). Electrons-rich or electrons-poor zone could being discriminated over the whole molecule, to design the favorable attack mechanism. Nucleophilic, electrophilic and neutral features were calorimetrically displayed by red, blue and green colors, respectively. It is easily to notice nucleophilicity of O(11), O(13) and N(16) centers in the free ligand. These atoms were the coordinating sites which appeared by the same nucleophilic feature in all complexes but improved in Cu(II) and Ni(II) complexes due to M→L charge transfer [54].

3.9. Biological simulation studies

3.9.1. Pharmacophore profile

To build interactive environment which leads to recognize virtual interaction for tested compounds with biological systems as well as create pharmacophore quires to reach analogues drug, Pharmit link must be used. This docking approach was done according to type of ligand-based *via* grid-based, to indicate the interaction ability of each tested compound with 1kzy and 6va5 as PDB proteins. The two proteins selected for this study belong DNA and their assignments were exhibited in Scheme 1S. As we know, the controlling of DNA in pathogenic-cells, is a significant target for treatment due to the role of DNA in growth.

Such *in-silico* way showed significant interactions with 6va5 protein (Fig. 6) which exceeded than that with other protein (1kzy, Fig. 14S). The complexes Ni(II)-Bis(HL) and Co(II)-Bis(HL) exhibited a very good occlusion in 6va5-grooves which yielded a perfect interaction in between. This interaction was carried out by high number of H-bonds as, H-donor (H-don =5), H-acceptor (H-acc=6), acidic (H-acid=0) and basic (H-based=1) with the two complexes. Moreover and it is worthy to note that, pharmacophore query was run through MolPort drug library [55] to obtain drug-like that showed effective interaction with 6va5 and 1kzy proteins. The drug model (No: MolPort-007–588–377) that showed activity towards 6va5 protein (Scheme 3) nears to tested hydrazide, was obtained. Its Room-Mean-Square deviation (RMSD), which measures the average distance between the atoms inside the ligand and protein receptors, is very low (0.012) to a favorable extent. Also, the drug model (No: MolPort-000–734–772) showed activity towards 1kzy protein (Scheme 3) nears to tested ligand, was obtained. Its Room-Mean-Square deviation (RMSD) is relatively low (0.198) [56].

3.9.2. Molecular docking approach

Molecular operating environmental docking-module (MOE) was used to simulate what happened inside pathogenic-cell after treatment by these new compounds, what is the interaction features towards DNA. This simulation technique is strongly recommended by drug designing industry, according to high credibility of resulting data which throw a shadow on the preferable design for targeted drug. The activity of new compounds was tested versus to 6va5 and 1kzy proteins, to measure the extent of DNA- controlling, as the first target of chemotherapy. Pharmacophore profile estimated in the previous step, gave the probability for these compounds to be succeeded in controlling DNA-proteins and high analogist with known drugs. Whereas, this docking tool gives all interaction details between the tested compounds and target proteins, which conducts to evaluate their potential drug behavior (Table 5, Figs. 7, 15S-17S). The docking processes consumed variable times from case to another till reach the most stable docking poses [57].

All interaction patterns obtained (Figs. 8, 15S-17S) are only for true docking poses in which the lengths of H-bonding formed agree with defined limit ($\leq$ 3.5 Å). Consequently, the Scoring values were the measurable limit for effectiveness of tested compounds towards the chosen proteins (6va5 & 1kzy). The comparative view for the data yielded from docking study, leads to the following significances;

1 The scoring energy values with all studied compounds were appeared moderate, except Co(II)-Bis(HL) and Ni(II)-Bis(HL) complexes with the two proteins, their values appeared high(from −6.5028 to −7.037). This predicts the biological effectiveness of the two complexes in controlling pathogenic cell-DNA.
2 The ligitional sites were O11, 12, 17, 18, 81 & 83 and N15, 21, 38 & 22 that interacted with protein pockets through allosteric H-donor or H-acceptor, mainly.
3 The interacting receptors and dummies were the following amino acid residues; ARG1490, 1595, 282; SER116, 96; GLU117, 1598, 1543, 1567, 262, 258 and ASP208.
4 The polar receptors that appeared as a pink circle were interacting as backbone or side chain, while the nonpolar receptors (green circle) were completely absent from all interaction types (Figs 15S & 16S).
5 The ligand exposure surface was appeared lower with most interacting compounds towards 6va5 protein. While, such surface was appeared broad in interaction patterns with 1kzy protein. This denotes the high degree of unsaturation for interacting sites which could make extra bonding with 1kzy receptors. This observation harmonized with the appearance of proximity contour (dotted line surrounds the compound) (Figs 15S & 16S).
6 The inhibition superiority of Co(II)-Bis(HL) and Ni(II)-Bis(HL) complexes that strongly concluded, may refer to presence of Bis-ligand which offer doublet donor numbers which capable for extra binding with protein-pockets [58]. This behavior was predicated in previous part (3.8.2) from molecular modeling results.
7 The energy content appeared lower to preferable limit with the two reported complexes till −17.9 and −12.1 Kcal/mol, respectively (Table 5) [58].
8 Broad electrostatic surface of docking proteins (Figs. 7& 17S), that observed with most complexes, indicates well penetration for such complexes inside DNA-grooves that obtained from helix deterioration during interaction.

3.10. Biological application

3.10.1. Antimicrobial activity

Three microbial strains used in this investigation were *Staphylococcus aureus* (*G*+ve), *E. coli* (G-ve) and *Candida albicans* (fungi). They were commercially available from Microbiology laboratory of national organization for drug control and research (NODCAR). This *in-vitro* assay was performed for all new compounds (Fig. 18S) to assess their antimicrobial efficiency. Significant effectiveness was the general feature remarked with compounds **5, 6** and **3**. This is according to the measured inhibition diameter zones as well as the activity index. This feature matches by acceptable extent with structural activity relationships reported, which indicates the lipophilicity of these compounds. Lipophilcity points to the ease of penetration in sebaceous membrane around the cell and then the direct attack with biological systems was happened [59]. Theoretically, we did not expect activity for compound **3** due to its high dipole moment value (11.526 Debye). But the in-vitro results indicate its high activity, this may be due to any unknown mechanism happened inside the cell and stimulate its activity [60].

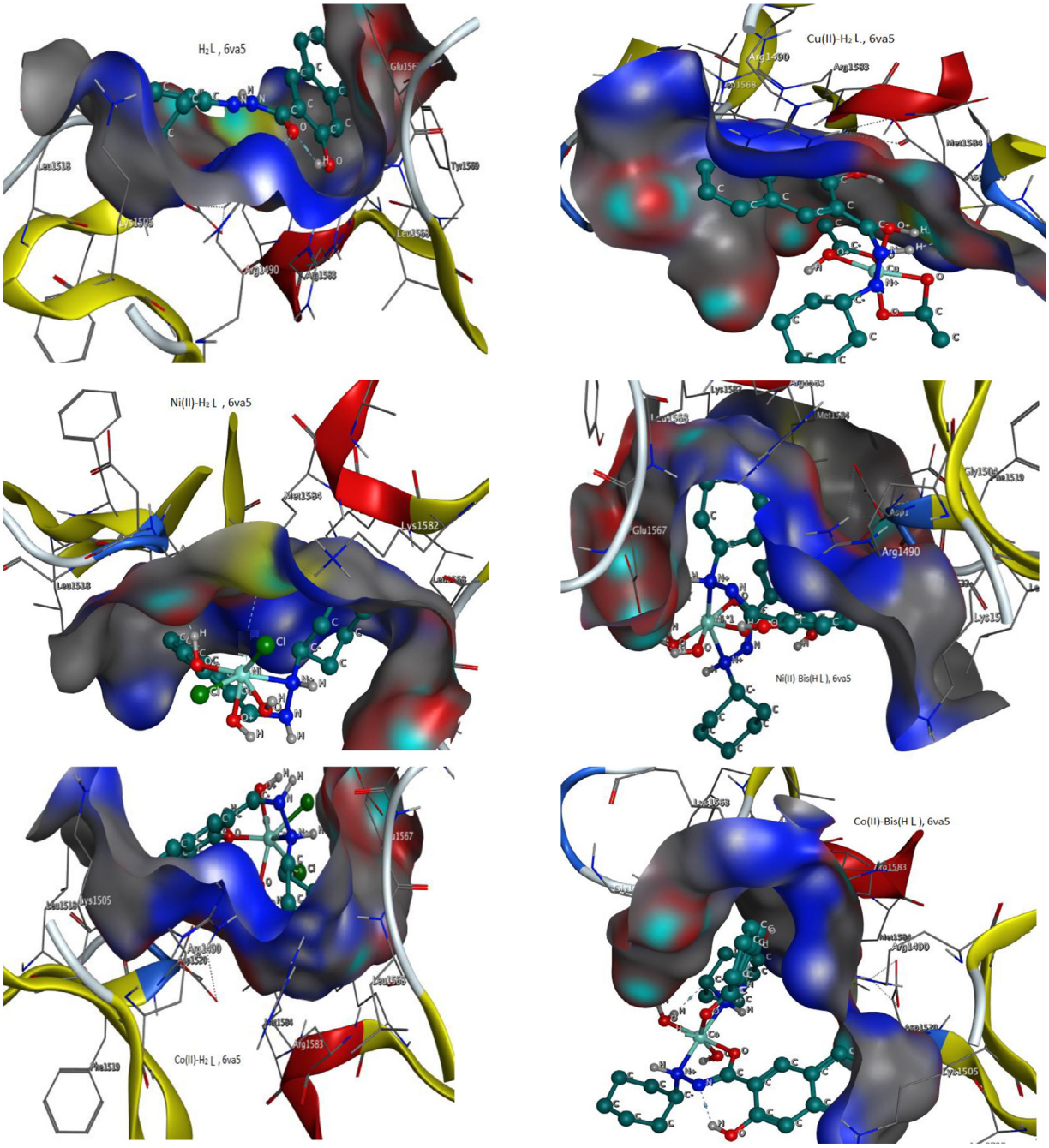

Fig. 7. Molecular surfaces for docking patterns obtained between synthesizes and 6va5 protein.

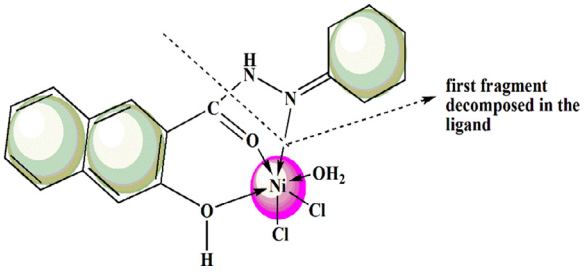

Scheme 2. The decomposition path in 3rd in TGA curve of the complex.

3.10.2. Antioxidant and cytotoxicity of new compounds

The antioxidant property of all compounds was examined by ABTS assay [61], to evaluate the magnitude of success in overcoming free radicals that initiates cancer cell-proliferation. Excellent antioxidant activity index (83.4%) was recorded with $[Ni(HL)_2(H_2O)_2]$ (**6**) complex which closer to the reference drug itself (ascorbic-acid) (Table 6S). This property of compound **6** may refer to its surprisingly lower dipole moment or polarity that concluded from computational study. Such pushed the compound to acquire electrons from surrounding and capable for trapping free radicals. Whereas, the free ligand exhibited mild antioxidant activity (57.23%), while the activity of other compounds seems ignored.

Cytotoxic property of the ligand and its complexes was examined against Hepatocellular carcinoma cell line (HepG2). This screening was compared with 5-fluorouracil (5-FU) as a positive

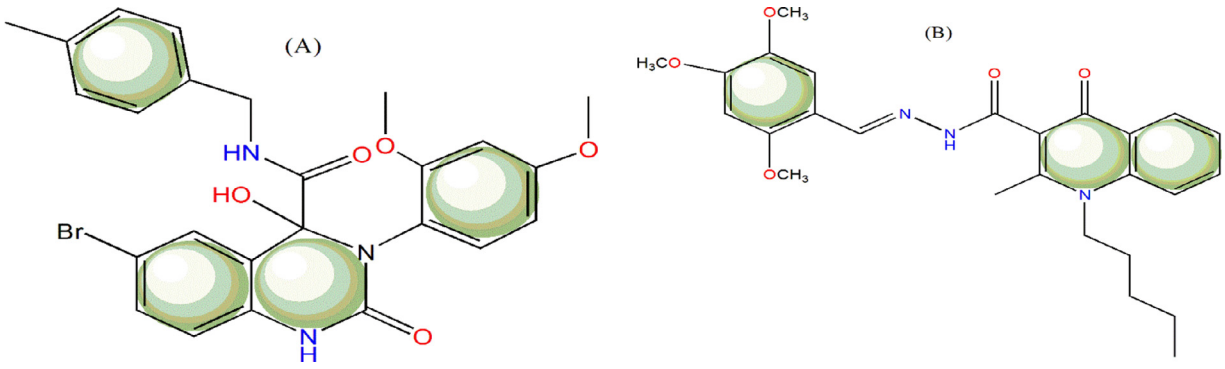

Scheme 3. drug-like conformers for H_2L ligand with 6va5 (A) and 1kzy (B) proteins.

Table 6
Cytotoxicity (IC50) of H_2L and its metal complexes on HepG2 cell line.

Compound	IC50(μg/ml)
5FU	2.6
1	3.6
2	7.9
3	7.4
4	10.2
5	9.3
6	8.7
7	2.9

control (reference) to obtain a broad view about their inhibition features [61]. IC_{50} values were evaluated and tabulated (Table 6). The values reflect the superiority of compound **7** (2.9 μg/ml) in its antitumor behavior which compatible with that of standard drug (2.6 μg/ml). While, the free ligand takes the second order in its inhibition activity by IC_{50} value =3.6 μg/ml [62]. Consequently, the two compounds may have distinguished future in fighting this disease.

Finally it easily to remark that, the chemical features and activity of complexes are changed strongly by changing the conjugated anions in metal salts used to form complexes, even with the same ligand.

4. Conclusion

New hydrazide complexes were prepared by green strategy from $CuSO_4$, $Cu(OAc)_2$, $NiCl_2{\cdot}6H_2O$, $Ni(OAc)_2{\cdot}4H_2O$, $CoCl_2{\cdot}6H_2O$ and $Co(OAc)_2{\cdot}4H_2O$ salts, to assert on the changes in their characteristics according to different anions. The ligand behaved as a neutral or monobasic through bidentate or tridentate binding mode towards the metal ions within different molar ratios (1: 1 or 1:2, M:L). This suggestion was confirmed from analytical and spectroscopic studies that implemented for characterization. Conductometric measurements were used to calculate the association and formation constants for Co(II)-ligand complex which formed by 1:2 molar ration. Material studio package was used to optimize the structural forms and then confirms the mode of bonding through the changes observed in bond lengths and angles. Drug-likeness approach was applied to discover pharmacophore profile within MolPort drug-library. Two drugs were discovered as analogues for the tested compounds in the activity towards DNA proteins (6va5 and 1kzy). This outcomes were confirmed and elaborated by other *in-silico* way as MOE-docking. The data point to Co(II)-Bis(HL) and Ni(II)-Bis(HL) complexes as the most favorable inhibitors that could control DNA of pathogenic cells. Finally, antimicrobial, antioxidant and antitumor activity were tested for all compounds and Ni(II)-Bis(HL) complex showed excellent antioxidant property, while Co(II)-Bis(HL) complex showed superior cytotoxicity towards liver cancer cells. Finally, the whole characteristics of complexes were changed by changing conjugated anions, even with the same ligand.

Declaration of Competing Interest

The authors declare that they have no known competing financial interests or personal relationships that could have appeared to influence the work reported in this paper.

Acknowledgement

Taif University Researchers Supporting Project number (TURSP-2020/14), Taif University, Taif, Saudi Arabia

Supplementary materials

Supplementary material associated with this article can be found, in the online version, at doi:10.1016/j.molstruc.2021.130410.

References

[1] a) L.H. Abdel-Rahman, N.M. Ismail, M. Ismael, A.M. Abu-Dief, E.A. Ahmed, Synthesis, characterization, DFT calculations and biological studies of Mn (II), Fe (II), Co (II) and Cd (II) complexes based on a tetradentate ONNO donor Schiff base ligand, J.Mol. Struct. 1134 (2017) 851–862; b) L.H. Abdel-Rahman, M.S. Adam, A.M. Abu-Dief, H. Moustafa, M. Basha, A.H. Aboria, B. Saad Al–Farhan, H.E. Ahmed, Synthesis, theoretical investigations, biocidal screening, DNA binding, in vitro cytotoxicity and molecular docking of novel Cu (II), Pd (II) and Ag (I) complexes of chlorobenzylidene Schiff base: promising antibiotic and anticancer agents, Appl Organomet. Chem. 32 (2018) e4527; c) L.H. Abdel-Rahman, A.M. Abu-Dief, A.A.H. Abdel-Mawgoud, Development, structural investigation, DNA binding, antimicrobial screening and anticancer activities of two novel quari-dentate VO (II) and Mn (II) mononuclear complexes, J. King. Saud Uni 31 (1) (2019) 52; d) L.H. Abdel-Rahman, A.A. Abdelhamid, A.M. Abu-Dief, M.R. Shehata, M.A. Bakheet, Facile synthesis, X-Ray structure of new multi-substituted aryl imidazole ligand, biological screening and DNA binding of its Cr (III), Fe (III) and Cu (II) coordination compounds as potential antibiotic and anticancer drugs, J. Mol. Struct. 1200 (2020) 127034.
[2] G. A.A.Al-Hazmi, N. El-Metwally, A series of nickel(II) complexes derived from hydrazide derivatives, electrochemical, thermal and spectral studies, Arabian Journal of Chemistry 10 (2017) S1003–S1013.
[3] H. Katouah, A.M. Hameed, A. Alharbi, F. Alkhatib, R. Shah, S. Alzahrani, R. Zaky, N.M. El-Metwaly, Green Synthesis Strategy for New Schiff-Base Complexes: characterization, Conductometry, Vitro Assay Confirmed by In Silico Approach, ChemistrySelect 5 (33) (2020) 10256–10268.
[4] H.A. Katouah, J.H. Al-Fahemi, M.G. Elghalban, F.A. Saad, I.A. Althagafi, N.M. El-Metwaly, A.M. Khedr, Synthesis of new Cu (II)-benzohydrazide nanometer complexes, spectral, modeling, CT-DNA binding with potential anti-inflammatory and anti-allergic theoretical features, Mater. Sci. Eng.: C 96 (2019) 740–756.
[5] B. Fisher, R. Eisenberg, Electrocatalytic reduction of carbon dioxide by using macrocycles of nickel and cobalt, J. Am. Chem. Soc. 102 (1980) 7361–7363.

[6] F. Alkhatib, A. Hameed, A. Sayqal, A.A. Bayazeed, S. Alzahrani, Z.A. Al-Ahmed, R. Zaky, N.M. El-Metwaly, Green-synthesis and characterization for new Schiff-base complexes; spectroscopy, conductometry, Hirshfeld properties and biological assay enhanced by in-silico study Arab, J. Chem. 13 (8) (2020) 6327–6340.

[7] Sh.M. Morgan, A.Z. El-Sonbati, H.R. Eissa, Geometrical structures, thermal properties and spectroscopic studies of Schiff base complexes: correlation between ionic radius of metal complexes and DNA binding, J. Mol. Liq. 240 (2017) 752–776.

[8] R. Shah, H. Katouah, A.A. Sedayo, M. Abualnaja, M.M. Aljohani, F. Saad, R. Zaky, N.M. El-Metwaly, Practical and computational studies on novel Schiff base complexes derived from green synthesis approach: conductometry as well as in-vitro screening supported by in-silico study, J. Mole. Liquids 319 (2020) 114116.

[9] B. Tamami, S. Ghasemi, Catalytic activity of Schiff-base transition metal complexes supported on crosslinked polyacrylamides for hydrogen peroxide decomposition, J. Organomet, Chem. 794 (2015) 311–317.

[10] R. Antony, S.T. David, K. Saravanan, K. Karuppasamy, S. Balakumar, Synthesis, spectrochemical characterisation and catalytic activity of transition metal complexes derived from Schiff base modified chitosan, Spectrochim Acta A 103 (2013) 423.

[11] S. Shen, H. Chen, T. Zhu, X. Ma, J. Xu, W. Zhu, R. Chen, J. Xie, T. Ma, L. Jia, Y. Wang, C. Peng, Synthesis, characterization and anticancer activities of transition metal complexes with a nicotinohydrazone ligand, Oncology Lettersm 13 (5) (2017) 3169–3176.

[12] S. Alzahrani, M. Morad, A. Bayazeed, M. Aljohani, F. Alkhatib, R. Shah, H. Katouah, H.M. Abumelha, I. Althagafi, R. Zaky, N.M. El-Metwaly, Ball milling approach to prepare new Cd (II) and Zn (II) complexes; characterization, crystal packing, cyclic voltammetry and MOE-docking agrees with biological assay, J. Mol. Struct 1218 (2020) 128473.

[13] H. Katouah, A. Sayqal, A.M. Al-Solimy, H.M. Abumelha, R. Shah, F. Alkhatib, S. Alzahrani, R. Zaky, N.M. El-Metwaly, Facile synthesis and deliberate characterization for new hydrazide complexes; cyclic voltammetry, crystal packing, eukaryotic DNA degradation and in-silico studies, J. Mol. Liq. 320 (2020) e114380.

[14] H.M. Abumelha, J.H. Al-Fahemi, I. Althagafi, A.A. Bayazeed, Z.A. Al-Ahmed, A.M. Khedr, N. El-Metwaly, Deliberate-characterization for Ni (II)-Schiff base complexes: promising in-vitro anticancer feature that matched MOE docking-approach, J. Inorg. Organomet Polym (2020) 1–17.

[15] R. Shah, A. Alharbi, A.M. Hameed, F. Saad, R. Zaky, A.M. Khedr, N. El-Metwaly, Synthesis and structural elucidation for new Schiff base complexes; conductance, conformational, MOE-docking and biological studies, J. Inorg. Organomet Polym (2020) 1–13.

[16] G.A.A. Al-Hazmi, K.S. Abou-Melha, N.M. El-Metwaly, I. Althagafi, F. Shaaban, R. Zaky, Green synthesis approach for Fe (III), Cu (II), Zn (II) and Ni (II)-Schiff base complexes, spectral, conformational, MOE-docking and biological studies, Appl. Organomet Chem. 34 (3) (2020) e5403.

[17] A.S. Al-Wasidi, A.M. Naglah, M.A. Al-Omar, A.M. Al-Obaid, E.H. Alosaimi, N.M. El-Metwaly, M.S. Refat, A.S. Ahmed, I.M. El-Deen, A.H. Soliman, A. Emam, Manganese (II), ferric (III), cobalt (II) and copper (II) thiosemicarbazone Schiff base complexes: synthesis, spectroscopic, molecular docking and biological discussions, Materials Express 10 (2) (2020) 290–300.

[18] G.A.A. Al-Hazmi, K.S. Abou-Melha, N.M. El-Metwaly, I. Althagafi, F. Shaaban, M.G. Elghalban, M.M. El-Gamil, Spectroscopic and theoretical studies on Cr (III), Mn (II) and Cu (II) complexes of hydrazone derived from picolinic hydrazide and O-vanillin and evaluation of biological potency, Appl. Organomet. Chem. 34 (3) (2020) 5408.

[19] G.A.A. Al-Hazmi, K.S. Abou-Melha, N.M. El-Metwaly, I. Althagafi, R. Zaki, F. Shaaban, Green synthesis for 3-(2-benzoylhydrazono)-N-(pyridin-2-yl) butanamide complexes: spectral, analytical, modelling, MOE docking and biological studies, J. Inorg. Organomet. Polym. (2019) 1–18.

[20] *Modeling and Simulation Solutions For Chemicals and Materials Research*, Materials Studio (Version 5.0), Accelrys software Inc., San Diego, USA, 2009 Available online at: www.accelrys.com.

[21] C. Lee, W. Yang, R.G. Parr, Development of the Colle-Salvetti correlation-energy formula into a functional of the electron density, Physical review B 37 (2) (1988) 785–789.

[22] W.J. Hehre, L. Radom, P.V.R. Schlyer, J.A. Pople, Ab Initio Molecular Orbital Theory, Wiley, New York, 1986, doi:10.1002/jcc.540070314.

[23] A. Kessi, B. Delley, Density functional crystal vs. cluster models as applied to zeolites, Int. J. Quantum Chem. 68 (1998) 135–144.

[24] C.D. Willey, J.A. Bonner, Interaction of chemotherapy and radiation Gunderson LL, Tepper JEBT-CRO (Third E, editors. Clin. Radiat. Oncol. 3rd Editio, Philadelphia: W.B. Saunders); 2012; 65–82.

[25] J. Sunseri, D.Ryan Koes, Pharmit: interactive exploration of chemical space, J. Pharmit, *Nucleic Acids Research* 44 (W1) (2016) W442–W448.

[26] T.M. Musyoka, A.M. Kanzi, K.A. Lobb, Ö.T. Bishop, Structure based docking and molecular dynamic studies of plasmodial cysteine proteases against a South African natural compound and its analogs, Sci Rep 6 (2016) 1–12.

[27] S.Y. Al-nami, E. Aljuhani, I. Althagafi, H.M. Abumelha, T.M. Bawazeer, A.M. Al–Solimy, Z.A. Al-Ahmed, F. Al-Zahrani, N. El-Metwaly, Synthesis and Characterization for new nanometer Cu (II) complexes, conformational study and molecular docking approach compatible with promising in vitro screening, Arab. J. Sci. Eng. (2020) 1–18.

[28] N. El-Metwaly, I. Althagafi, A.M. Khedr, J.H. Al-Fahemi, H.A. Katouah, A.S. Hossan, A.Y. Al-Dawood, G.A. Al-Hazmi, Synthesis and characterization for novel Cu (II)-thiazole complexes-dyes and their usage in dyeing cotton to be special bandage for cancerous wounds, J. Mol. Struct.1194. (2019) 86–103.

[29] M. Balouiri, M. Sadiki, S.K. Ibnsouda, Methods for in vitro evaluating antimicrobial activity: a review, J. Pharm. Anal. 6 (2) (2016) 71–79.

[30] E. Lissi, B. Modak, R. Torres, J. Escobar, A. Urza, Total antioxidant potential of resinous exudates from Heliotropium species, and a comparison of the ABTS and DPPH methods, Free Radic. Res. 30 (1999) 471.

[31] R. Aeschlach, J. Loliger, C.B. Scott, A. Murcia, J. Butler, B. Halliwel, I.O. Aruoma, Antioxidant actions of thymol, carvacrol, 6-gingerol, zingerone and hydroxytyrosol, Food Chem. Toxicol. 32 (1994) 31–36.

[32] W.J. Geary, The use of conductivity measurements in organic solvents for the characterisation of coordination compounds, Coordin. Chem. Rev. 7 (1971) 81–122.

[33] K. Nakamoto, Infrared Spectra of Inorganic and Coordination Compounds, Wiley, New York, 1970.

[34] R.K. Shah, K.S. Abou-Melha, F.A. Saad, T. Yousef, G.A.A. Al-Hazmi, M.G. Elghalban, A.M. Khedr, N. El-Metwaly, Elaborated studies on nano-sized homo-binuclear Mn(II), Fe(III), Co(II), Ni(II), and Cu(II) complexes derived from N_2O_2 Schiff base, thermal, molecular modeling, J. Therm. Anal. Calorim. 123 (1) (2016) 731–743.

[35] J.H. Al-Fahemi, F.A. Saad, N.M. El-Metwaly, T.A. Farghaly, M.G. Elghalban, K.A. Saleh, G.A. Al-Hazmi, Synthesis of Co(II), Cu(II), Hg(II), UO_2(II) and Pb(II) binuclear nanometric complexes from multi-donor ligand: spectral, modeling, quantitative structure–activity, Appl. Organomet. Chem. 31 (11) (2017) e3787.

[36] A.B.P. Lever, Inorganic Electronic Spectroscopy, Elsevier, Amsterdam, 1968.

[37] R. Shah, T.M. Habeebullah, F. Saad, I. Althagafi, A.Y. Al-dawood, A.M. Al-Solimy, Z.A. Al-Ahmed, F. Al-Zahrani, T.A. Farghaly, N. El-Metwaly, Characterization of new Co (II) complexes and photographic monitoring for their toxic impact on breast cancer cells according to simulation study, Appl. Organomet. Chem. 34 (10) (2020) e5886.

[38] A.A. Abou-Hussen, N.M. El-Metwaly, E.M. Saad, A.A. El-Asmy, Spectral, magnetic, thermal and electrochemical studies on phthaloyl bis (thiosemicarbazide) complexes, J. Coord. Chem. 58 (2005) 1735–1749.

[39] B.J. Hathaway, A new look at the stereochemistry and electronic properties of complexes of the copper(II) ion, Complex Chemistry (2007) 55–118.

[40] K.S. Abu-Melha, N.M. El-Metwally, Spectral and thermal studies for some transition metal complexes of bis (benzylthiocarbohydrazone) focusing on EPR study for Cu (II) and VO^{2+}, Spectrochimica Acta Part A 70 (2) (2008) 277.

[41] J.A. Welleman, F.B. Hulsbergen, Influence of alkyl chain length in N-alkyl imidazoles upon the complex formation with transition-metal salts, J. Inorg. Nucl. Chem. 40 (1978) 143–147.

[42] M. Shakir, S. Hanif, M.A. Sherwani, O. Mohammad, S.I. Al-Resayes, Pharmacologically significant complexes of Mn (II), Co (II), Ni (II), Cu (II) and Zn (II) of novel Schiff base ligand,(E)-N-(furan-2-yl methylene) quinolin-8-amine: synthesis, J. Mol. Struct. 1092 (2015) 143–159.

[43] F.A. Saad, N.M. El-Metwaly, A.M. Khedr, Synthesis, characterization for new nanometric VO (II)–thioacetanilide complexes by, spectral, thermal, molecular computations and DNA interaction study beside promising, J. Inorg. Organomet. Polym. 29 (2019) 1606–1624.

[44] M.S. Refat, N.M. El-Metwaly, Spectroscopic and fluorescence studies on Mn (II), Co (II), Ni (II) and Cu (II) complexes with NO donor fluorescence dyes, Spectrochim, Acta A Mol. Biomol. Spectrosc 81 (2011) 215–256.

[45] B.D. Cullity, Elements of X–Ray Diffraction, 2nd edn., Addison–Wesley Inc., 1993.

[46] K. Momma, F. Izumi, VESTA 3 for three-dimensional visualization of crystal, volumetric and morphology data, J. Appl. Crystallogr. 44 (2011) 1272–1276.

[47] a) A.W. Coats, J.P. Redfern, Kinetic Parameters from Thermogravimetric DataNature 20 (1964) 68; b) L.H. Abdel-Rahman, A.M. Abu-Dief, M. O.Aboelez, A.A.H. Abdel-Mawgoud, DNA interaction, antimicrobial, anticancer activities and molecular docking study of some new VO (II), Cr (III), Mn (II) and Ni (II) mononuclear chelates encompassing quaridentate imine ligand, J. Photochem. Photobiol. B. 170 (2017) 271; c) A.M. Abu-Dief, L.H. Abdel-Rahman, A.A. Abdelhamid, A.A. Marzouk, M.R. Shehata, M. Abdelaal Bakheet, O.A. Almaghrabi, A. Nafady, Synthesis and characterization of new Cr (III), Fe (III) and Cu (II) complexes incorporating multi-substituted aryl imidazole ligand: structural, DFT, DNA binding, and biological implications, Spectrochimica Acta Part A 228 (2020) 117700.

[48] H.W. Horowitz, G.A. Metzger, A New Analysis of Thermogravimetric Traces, Anal. Chem. 35 (1963) 1464–1468.

[49] I. Althagafi, M.G. Elghalban, N.M. El–Metwaly, Novel synthesized benzesulfonamide nanosized complexes; spectral characterization, molecular docking, molecular modeling and analytical application, J. Inorg. Organomet. Polym. 29 (3) (2019) 876–892.

[50] F.A. Saad, J.H. Al-Fahemi, H. El-Ghamry, A.M. Khedr, M.G. Elghalban, N.M. El-Metwaly, Elaborated spectral, modeling, QSAR, docking, thermal, antimicrobial and anticancer activity studies for new nanosized metal ion complexes derived from sulfamerazine azodye, J. Therm. Anal. Calorim 131 (2018) 1249–1267.

[51] N.A. El-Shishtawi, M.A. Hamada, E.A. Gomaa, Influence of permanent magnet on the association constants of $FeCl_3$ in 50% ethanol-H2O solutions(conductometrically) at 298.15 K using a new equation for 1:3 asymmetric electrolytes, J. Chem. Eng. Data 55 (2010) 5422.

[52] K.M. Ibrahim, E.A. Gomaa, R.R. Zaky, S.M. Abo-Zeid, The Association and Formation Constants for Co(II), Ni(II) and Cu(II) with (H2SHAH) in Mixed Solvents at 290.15 K AASCIT, J. Chem. 2 (2015) 48.

[53] A.Y. Al-Dawood, N.M. El-Metwaly, H.A. El-Ghamry, Molecular docking and DFT studies on some nano-meter binuclear complexes derived from hydrazine-carbothioamide ligand, synthesis, thermal, kinetic and spectral characterization, J. Mol. Liq. 220 (2016) 311–323.
[54] F.A. La Porta, T.C. Ramalho, R.T. Santiago, M.V.J. Rocha, E.F.F. da Cunha, Orbital signatures as a descriptor of regioselectivity and chemical reactivity: the role of the frontier orbitals on 1, 3-dipolar cycloadditions, J. Phys. Chem. 115 (2011) 824.
[55] P. Mu, R. Karuppasamy, Discovery of human autophagy initiation kinase ULK1 inhibitors by multi-directional *in silico* screening strategies, J. Receptors and Signal Transduction 39 (2) (2019) 122–133.
[56] N. Kandakatla, G. Ramakrishnan, Ligand based pharmacophore modeling and virtual screening studies to design novel HDAC2 inhibitors Adv, Bioinforma 2014 (2014) 812148.
[57] A.S. Obrecht, N. Urban, M. Schaefer, A. Röse, A. Kless, J.E. Meents, A. Lampert, A. Abdelrahman, C.E. Müller, G. Schmalzing, R. Hausmann, Identification of aurinitricarboxylic acid as a potent allosteric antagonist of P2X1 and P2X3 receptors, Neuropharmacology 158 (2019) 107749.
[58] G.A.A. Al-Hazmi, K.S. Abou-Melha, I. Althagafi, N.M. El-Metwaly, F. Shaaban, M.S. Abdul Galil, A.A. El-Bindary, Synthesis and structural characterization of oxovanadium (IV) complexes of dimedone derivatives, Appl. Organomet. Chem. (2020) e5672.
[59] N.M. El-Metwaly, M.S. Refat, Spectral, thermal, kinetic, molecular modeling and eukaryotic DNA degradation studies for a new series of albendazole (HABZ) complexes, Spectrochim. Acta A. 81 (2011) 519–528.
[60] A.A.A. Emara, A.A. Saleh, O.M.I. Adly, Spectroscopic investigations of new binuclear transition metal complexes of Schiff bases derived from 4,6-diacetylresorcinol and 3-amino-1-propanol or 1,3-diamino-propane, Spectrochim. Acta A. 68 (2007) 592–604.
[61] T. Rosu, A. Gulea, A. Nicolae, R. Georgescu, omplexes of $3d^n$ Metal Ions with Thiosemicarbazones: synthesis and Antimicrobial Activity, Molecules 12 (2007) 782–796.
[62] A.M. Abu-Dief, H.M. El-Sagher, M.R. Shehata, Fabrication, spectroscopic characterization, calf thymus DNA binding investigation, antioxidant and anticancer activities of some antibiotic azomethine Cu (II), Pd (II), Zn (II) and Cr (III) complexes, Appl. Organomet. Chem. 33 (8) (2019) e4943.